

CERN-PH-EP-2014-196
29 July 2014

Production of inclusive $\Upsilon(1S)$ and $\Upsilon(2S)$ in p–Pb collisions at $\sqrt{s_{NN}} = 5.02$ TeV

ALICE Collaboration*

Abstract

We report on the production of inclusive $\Upsilon(1S)$ and $\Upsilon(2S)$ in p–Pb collisions at $\sqrt{s_{NN}} = 5.02$ TeV at the LHC. The measurement is performed with the ALICE detector at backward ($-4.46 < y_{\text{cms}} < -2.96$) and forward ($2.03 < y_{\text{cms}} < 3.53$) rapidity down to zero transverse momentum. The production cross sections of the $\Upsilon(1S)$ and $\Upsilon(2S)$ are presented, as well as the nuclear modification factor and the ratio of the forward to backward yields of $\Upsilon(1S)$. A suppression of the inclusive $\Upsilon(1S)$ yield in p–Pb collisions with respect to the yield from pp collisions scaled by the number of binary nucleon-nucleon collisions is observed at forward rapidity but not at backward rapidity. The results are compared to theoretical model calculations including nuclear shadowing or partonic energy loss effects.

*See Appendix A for the list of collaboration members

1 Introduction

Quarkonia are bound states of a heavy quark and its anti-quark. The J/ψ family is comprised of charm and anti-charm quarks and the Υ family of bottom and anti-bottom quarks. The former are commonly called charmonia and the latter bottomonia. In elementary pp collisions, the production of a quarkonium can be understood as the creation of a heavy-quark pair ($Q\bar{Q}$) followed by its binding into a quarkonium state with given quantum numbers [1]. The first step is well described by perturbative quantum chromodynamics (QCD) while the second step is inherently non-perturbative. Three main approaches are used to describe quarkonium production in hadronic collisions: the Color Evaporation Model (CEM) [2, 3], the Color-Singlet Model (CSM) [4] and the Non-Relativistic QCD (NRQCD) framework [5]. However, none of those models is able to satisfactorily describe simultaneously all aspects of quarkonium production in pp collisions [6].

In ultra-relativistic Pb–Pb collisions, quarkonia are important probes to study the properties of the deconfined state of partonic matter, the quark-gluon plasma (QGP). Such a state is predicted by QCD at high temperature and pressure [7, 8]. Since quarkonia are produced at the early stage of the collision, they are expected to interact with the QGP throughout its evolution. In particular, in the colour-screening scenario [9] quarkonium states are suppressed in the QGP with different dissociation probabilities for the various mass states, depending on their binding energy. The CMS Collaboration at the Large Hadron Collider (LHC) has reported on the observation of the sequential suppression of bottomonium states in Pb–Pb collisions at $\sqrt{s_{NN}} = 2.76$ TeV [10, 11]. However, other hot nuclear matter effects besides colour screening, as well as cold nuclear matter (CNM) effects, do complicate this simple picture. On the one hand, recent measurements by the ALICE Collaboration are compatible with a regeneration mechanism playing an important role in the production of J/ψ in Pb–Pb collisions at the LHC [12–14]. Additional J/ψ are expected to be produced from deconfined charm quarks by kinetic recombination in the QGP [15, 16] or by statistical hadronization at the phase boundary [17]. This additional, hot nuclear matter effect, competes with the suppression by colour screening. Due to the lower production cross section of $b\bar{b}$ pairs compared to $c\bar{c}$ pairs, the regeneration of $\Upsilon(1S)$ is expected to be smaller than that of J/ψ [18]. On the other hand, effects related to the presence of CNM can also modify the production of quarkonia in nucleus-nucleus collisions.

Cold nuclear matter effects can be separated into initial and final-state effects. Initial-state effects occur prior to the formation of the heavy-quark pair. These include the modification of the kinematical distribution of the partons in the nuclei compared to that in free nucleons [19–22] as well as parton energy loss mechanism [23–25]. First, the nuclear Parton Distribution Functions (nPDF) differ from those in free nucleons (PDF). Since the gluon fusion mechanism dominates the production of heavy-quark pairs in high energy collisions, quarkonium production is particularly sensitive to the gluon nPDF, which is presently not well known. Bjorken- x (x_{Bj}) is defined as the fraction of the hadron momentum carried by the parton. The gluon nPDF includes a shadowing region at low x_{Bj} ($x_{Bj} \lesssim 0.01$) corresponding to a suppression of gluons, an antishadowing region at intermediate x_{Bj} ($0.01 \lesssim x_{Bj} \lesssim 0.3$) corresponding to an enhancement of gluons, and an additional suppression of gluons known as EMC effect at higher x_{Bj} ($0.35 \lesssim x_{Bj} \lesssim 0.7$). Secondly, if the quarkonium production is dominated by low x_{Bj} gluons, then the Colour Glass Condensate (CGC) model can be used to describe the nucleus as a coherent gluonic system that saturates at very large density [26]. Finally, partons can lose energy before creating the heavy-quark pair, therefore modifying the kinematic distributions of quarkonia. Final-state effects are those that affect the heavy-quark pair during the finite time it needs to form a quarkonium state or after the state has been formed [27]. The $Q\bar{Q}$ pair can interact with the nuclear matter and eventually break-up. The break-up cross section depends on the nature of the pre-resonant state and is expected to be small for $\Upsilon(1S)$ at high energy [27, 28]. The final-state resonance can also interact with surrounding comovers and lose energy or even break-up. Finally, in a recent approach to parton energy loss [25], it is hypothesized that the parton energy loss is coherent and can not be factorized into initial and final state effects.

Cold nuclear matter effects can be studied in proton-nucleus (p–A) collisions where the QGP is not expected to be formed. Charmonium states have been extensively measured in p–A collisions at various collision energies up to LHC energies. Bottomonium production has recently been studied thanks to the increased energy and luminosity available in collider experiments at RHIC [29, 30] and the LHC [31]. Due to the larger mass of the bottomonium states compared to the charmonium ones, the measurement of Υ production in proton-nucleus collisions allows a study of cold nuclear matter effects in a different kinematic regime, therefore complementing the J/ψ studies [31–33]. In addition, the recent measurement by the ALICE Collaboration in Pb–Pb collisions of a stronger $\Upsilon(1S)$ suppression at forward rapidity [34] than at mid-rapidity has stressed the importance of understanding CNM effects on Υ production (since in the colour screening scenario such a behaviour is not expected as the energy density should be larger or equal at mid rapidity than at forward rapidity).

In this Letter, we report ALICE results on inclusive Υ production in p–Pb collisions at $\sqrt{s_{\text{NN}}} = 5.02$ TeV, measured via the $\mu^+\mu^-$ decay channel. The ALICE measurement of the $\Upsilon(1S)$ and $\Upsilon(2S)$ production cross section in p–Pb collisions at LHC energies is presented at backward ($-4.46 < y_{\text{cms}} < -2.96$) and forward ($2.03 < y_{\text{cms}} < 3.53$) centre-of-mass rapidities. The positive rapidity is defined by the direction of the proton beam. The $\Upsilon(1S)$ production cross sections in p–Pb collisions are compared to those in pp collisions scaled by the Pb-nucleus atomic mass number $A_{\text{Pb}} = 208$. This nuclear modification factor is presented as a function of rapidity. The ratio of the forward to backward yields is also discussed.

2 Experimental apparatus and data sample

The ALICE detector design and performance are extensively described in [35] and [36]. The analysis presented here is based on the detection of muons in the ALICE forward muon spectrometer, which covers the laboratory pseudorapidity range $-4 < \eta_{\text{lab}} < -2.5$. In addition, the Silicon Pixel Detector (SPD) is used to reconstruct the primary vertex, the VZERO detector provides a minimum bias trigger and the VZERO and TZERO detectors are both used as luminometers. A short description of these detectors is given in the following paragraphs.

The muon spectrometer consists of a set of absorbers, a dipole magnet with a 3 T·m field integral, five tracking stations and two trigger stations. The front absorber, made of carbon, concrete and steel and placed between 0.9 and 5 m from the Interaction Point (IP), filters out hadrons, thus decreasing the occupancy in the tracking system. Muon tracking is performed by five stations, each one consisting of two planes of Cathode Pad Chambers (CPC). The first two stations are located upstream of the dipole magnet, the third one is embedded inside the magnet gap and the fourth and fifth are placed downstream of the dipole, just before a 1.2 m thick iron wall (7.2 interaction lengths), which absorbs secondary hadrons escaping the front absorber and low-momentum muons (having $p < 1.5$ GeV/c at the exit of the front absorber). The muon trigger system is located downstream of the iron wall and consists of two stations, each one equipped with two planes of Resistive Plate Chambers (RPC). The time resolution is of the order of 2 ns and the efficiency is better than 95% [37]. The muon trigger system delivers single muon and dimuon triggers with a programmable transverse momentum (p_T) threshold. Throughout its entire length, a conical absorber around the beam pipe ($\theta < 2^\circ$) made of tungsten, lead and steel shields the muon spectrometer against secondary particles produced by the interaction of large- η primary particles in the beam pipe.

Primary vertex reconstruction is performed using the SPD, the two innermost layers of the Inner Tracking System [38]. It covers the pseudo-rapidity ranges $|\eta_{\text{lab}}| < 2$ and $|\eta_{\text{lab}}| < 1.4$, for the inner and outer layers respectively.

The two VZERO hodoscopes [39], with 32 scintillator tiles each, are placed on each side of the IP, covering the pseudo-rapidity ranges $2.8 < \eta_{\text{lab}} < 5.1$ and $-3.7 < \eta_{\text{lab}} < -1.7$. Each hodoscope is segmented into 8 sectors of equal azimuthal coverage and four equal pseudo-rapidity rings. The logical AND of the

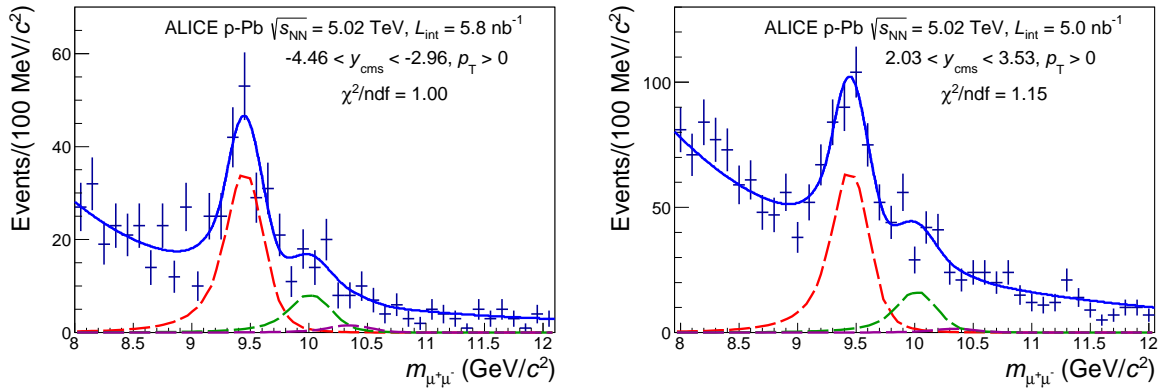


Fig. 1: Invariant mass distribution of opposite-sign dimuons in the rapidity regions $-4.46 < y_{\text{cms}} < -2.96$ (left) and $2.03 < y_{\text{cms}} < 3.53$ (right) in p–Pb collisions. In each case, the full curve shows the total fit function and the dashed curves the signal component for the three Υ states (see text for details).

signals from the two hodoscopes forms the Minimum Bias (MB) trigger, also used as a luminosity signal. A second luminosity signal is defined as the logical AND of the two TZERO arrays, located on opposite sides of the IP ($4.6 < \eta_{\text{lab}} < 4.9$ and $-3.3 < \eta_{\text{lab}} < -3.0$). Each array consists of 12 quartz Cherenkov counters, read by photomultiplier tubes.

The data samples used for this analysis were collected in 2013. The number of bunches colliding at the ALICE IP ranged from 72 to 288. The peak luminosity during data taking was about $10^{29} \text{ s}^{-1}\text{cm}^{-2}$. The average number of visible interactions per bunch crossing in such conditions is about 0.06, corresponding to a multiple interaction (pile-up) probability of about 3%.

The trigger condition used for data taking is a dimuon-MB trigger formed by the logical AND of the MB trigger and an unlike-sign dimuon trigger with a p_T threshold of 0.5 GeV/c for each of the two muons. The threshold is defined as the p_T value for which the single muon trigger efficiency is 50%. In an additional offline selection, the timing information of the two VZERO arrays is used to reject beam-halo and beam-gas events. The Zero Degree Calorimeters (ZDC), positioned symmetrically at 112.5 m from the IP, are used offline to reject events with a displaced vertex, originating from the interactions of satellite proton and lead bunches, as described in [36].

The two LHC beams have the same magnetic rigidity but different projectile charge to mass ratio, which results in the two beams having different energies: $E_p = 4 \text{ TeV}$ and $E_{\text{Pb}}/A_{\text{Pb}} = 1.58 \text{ TeV}$. As a consequence, the centre-of-mass system of nucleon–nucleon collisions is shifted in rapidity by $\Delta y = 0.465$ with respect to the laboratory frame in the direction of the proton beam. In terms of the rapidity in the centre-of-mass y_{cms} , the muon spectrometer acceptance is $2.03 < y_{\text{cms}} < 3.53$ when the proton beam is travelling in the direction of the spectrometer (p–Pb configuration), and $-4.46 < y_{\text{cms}} < -2.96$ in the opposite case (Pb–p configuration). To access both rapidity ranges, data were taken in the two configurations.

About 9.3×10^6 (2.1×10^7) dimuon-MB-triggered events were analysed for the p–Pb (Pb–p) configuration, corresponding to an integrated luminosity $\mathcal{L}_{\text{int}} = 5.01 \pm 0.19 \text{ nb}^{-1}$ ($5.81 \pm 0.20 \text{ nb}^{-1}$). The determination of the integrated luminosities and associated uncertainties are described later.

3 Data analysis

Muon track candidates are reconstructed in the muon spectrometer using the standard tracking algorithm [40]. The tracks are required to exit the front absorber at a radial distance from the beam axis, R_{abs} , in the range $17.6 < R_{\text{abs}} < 89.5 \text{ cm}$ to reject tracks crossing the region of the absorber with the highest

density material. In this region, multiple scattering and energy loss effects are large and can affect the mass resolution. The contribution from fake and beam-gas interaction induced tracks is reduced by selecting tracks pointing to the interaction vertex. In addition, tracks in the tracking system are requested to match a track segment in the trigger system (trigger tracklet).

The Υ signal is obtained from the invariant mass distributions of opposite-sign dimuons with a laboratory pair-rapidity in the range $2.5 < |y_{\text{lab}}| < 4$ down to zero transverse momentum. The raw number of Υ is obtained by fitting the invariant mass distributions. A sum of two exponential functions is used to parameterize the background continuum, and each Υ resonance shape is described by an extended Crystal Ball (CB) function [41]. The CB function is made of a Gaussian core and a power-law tail on each side and is found to reproduce the shape of the Υ peak obtained in Monte Carlo (MC) simulations. Since the CB tails are poorly constrained by the data, they are fixed from the results of the MC simulations. It is also necessary to fix the mass difference between states by using the PDG values [42] and to force the width of the $\Upsilon(2S)$ and $\Upsilon(3S)$ to scale proportionally with the $\Upsilon(1S)$ width according to the ratio of the resonance masses. MC simulations validated these assumptions. The $\Upsilon(1S)$ signal to background ratio (S/B)¹ is between 0.8 to 1.8, allowing the position and width of the $\Upsilon(1S)$ peak to be free parameters in the fit. The significance ($S/\sqrt{S+B}$) for $\Upsilon(1S)$ is between 6.3 and 11.6 for the rapidity bins considered in the analysis. The significance of the $\Upsilon(2S)$ in the rapidity ranges $-4.46 < y_{\text{cms}} < -2.96$ and $2.03 < y_{\text{cms}} < 3.53$ is larger than 3, which allows its measurement. However, due to the limited statistics, the significance of the $\Upsilon(3S)$ state is too low to separate the signal from the underlying background. Figure 1 illustrates the fitting method for the rapidity intervals $-4.46 < y_{\text{cms}} < -2.96$ (left panel) and $2.03 < y_{\text{cms}} < 3.53$ (right panel). The measured $\Upsilon(1S)$ peak position is in agreement with the resonance mass value from PDG [42] and the measured width (155 ± 25 MeV/ c^2 in $-4.46 < y_{\text{cms}} < -2.96$ and 160 ± 22 MeV/ c^2 in $2.03 < y_{\text{cms}} < 3.53$) with the results from MC simulations. The same agreement was observed for all rapidity bins considered in this Letter.

To investigate the systematic uncertainties on the signal extraction procedure, different fits were performed parameterizing the background continuum with the sum of two power-law functions and using alternative invariant mass fitting ranges. Since some parameters are fixed in the fitting procedure, the related systematic uncertainties were also studied. The CB tail parameters were varied according to their spread obtained by several fits of the MC distributions along different mass ranges. The width of the $\Upsilon(2S)$ and $\Upsilon(3S)$ were varied according to the size of the uncertainties of the $\Upsilon(1S)$ width obtained from the fit. The latter method was similarly used to estimate the systematic uncertainty related to the fixing of the $\Upsilon(2S)$ and $\Upsilon(3S)$ peak position. The raw number of $\Upsilon(1S)$ and $\Upsilon(2S)$ in the rapidity range $-4.46 < y_{\text{cms}} < -2.96$ are $161 \pm 21(\text{stat}) \pm 9(\text{syst})$ and $42 \pm 14(\text{stat}) \pm 5(\text{syst})$, respectively. In the $2.03 < y_{\text{cms}} < 3.53$ rapidity range, they are $305 \pm 34(\text{stat}) \pm 13(\text{syst})$ for $\Upsilon(1S)$ and $83 \pm 23(\text{stat}) \pm 10(\text{syst})$ for $\Upsilon(2S)$.

The acceptance-times-efficiency of the muon spectrometer for the measurement of Υ , $A \times \epsilon$, is calculated with MC simulations. The p_T and y distributions of the generated $\Upsilon(1S)$ were extrapolated, with a procedure equivalent to the one adopted for the J/ψ [43], to $\sqrt{s_{\text{NN}}} = 5.02$ TeV from existing pp measurements [44–46]. Nuclear shadowing calculations [47] were used to include the expected CNM effects. The systematic uncertainty was estimated by varying the p_T and y input distributions by an amount sufficiently large (based on theoretical estimations) to include the a priori unknown impact of CNM effects. Since the available data favour a zero or small polarization of $\Upsilon(1S)$ [48–50], an unpolarized production was assumed. Particle transport is performed using GEANT3 [51] and a realistic detector response is applied to the simulated hits in order to reproduce the performance of the apparatus during data taking. The time dependence of the tracking and trigger efficiencies are taken into account by incorporating in

¹The signal to background ratio and significance numbers are always evaluated at the three sigma level, *i.e.* the number of signal and background counts are evaluated in an invariant mass range centred on the Υ mass and corresponding to ± 3 times the width of the peak.

the MC simulations the dead channel maps obtained from the online detector information and the trigger chamber efficiencies obtained from a real data analysis. In addition, a realistic description of the residual misalignment of the tracking chambers is included in the simulations. The tracking efficiency is evaluated with data by analysing the cluster distribution of the reconstructed tracks in the detection chambers with the algorithm described in [40]. The same algorithm can be used to estimate the tracking efficiency from MC data. The systematic uncertainties on this value are obtained by comparing the tracking efficiency estimated from real and MC data. The efficiency of the muon triggering system is calculated from data and results from the analysis of trigger tracklet distribution reconstructed from clusters in the four planes of the two trigger stations. The corresponding systematic uncertainties are obtained by varying the trigger chamber efficiency in MC simulations by an amount equivalent to the statistical uncertainties on the real data estimation. The quality of the matching of the tracking and triggering system information is ensured by a χ^2 cut. In order to quantify the systematic uncertainties on the matching efficiency, the cut was varied in the same proportions while analysing both real and MC data. The observed difference in the matching probabilities provides the uncertainties.

The $A \times \epsilon$ values and the corresponding systematic uncertainties for $\Upsilon(1S)$ measured during the p–Pb and the Pb–p data taking periods are $(29.0 \pm 2.0)\%$ and $(20.1 \pm 1.6)\%$, respectively. The value of $A \times \epsilon$ is lower for the Pb–p period mainly due to a reduced tracking efficiency. The $\Upsilon(2S)$ $A \times \epsilon$ and the corresponding systematic uncertainties were evaluated with the same method and the same input distributions as for the $\Upsilon(1S)$. The observed differences between the $\Upsilon(2S)$ and $\Upsilon(1S)$ $A \times \epsilon$ are less than 0.5%. The shape variations between the different input distributions used in the study of the $A \times \epsilon$ systematic uncertainties were large enough to cover the differences between the $\Upsilon(1S)$ and $\Upsilon(2S)$ distributions observed by LHCb in the rapidity range $2 < y_{\text{cms}} < 4.5$ in pp collisions [45, 52, 53].

The raw number of $\Upsilon(1S)$ obtained with the fit procedure described previously, $N[\Upsilon(1S)]$, is corrected for the branching ratio of the dimuon decay channel, $\text{BR}_{\Upsilon(1S) \rightarrow \mu^+ \mu^-} = 0.0248 \pm 0.0005$ [42] and for the acceptance-times-efficiency, $(A \times \epsilon)_{\Upsilon(1S)}$. The $\Upsilon(1S)$ cross section is obtained as

$$\sigma_{\text{pPb}}^{\Upsilon(1S)} = \frac{N[\Upsilon(1S)] / (A \times \epsilon)_{\Upsilon(1S)}}{\text{BR}_{\Upsilon(1S) \rightarrow \mu^+ \mu^-} \times \mathcal{L}}, \quad (1)$$

where the integrated luminosity $\mathcal{L} = N_{\text{MB}} / \sigma_{\text{MB}}$ is the ratio between the number of MB events and the MB trigger cross section. Since the analysed data sample is made of dimuon triggered events, it is necessary to use a scaling factor, F , to obtain the number of MB events from the number of triggered events. The inverse of the F factor corresponds to the probability of having the dimuon trigger condition verified in a MB event. Its average value is $F = 1129 \pm 2(\text{stat}) \pm 11(\text{syst})$ and $F = 589 \pm 2(\text{stat}) \pm 6(\text{syst})$ for the p–Pb and Pb–p data taking periods, respectively. These values and the corresponding statistical uncertainties were obtained by averaging the results of two different methods, one based on the ratio of trigger rates and the other based on the offline selection of dimuon events in the MB data sample [32]. The systematic uncertainties reflect the difference obtained with the two methods. The MB trigger cross section σ_{MB} was measured with a van der Meer scan [54] and found to be 2.09 ± 0.07 b (2.12 ± 0.07 b) for the p–Pb (Pb–p) configuration, where the uncertainties for the two configurations are partially correlated [55]. The luminosity was also independently determined, in a similar way, by means of the TZERO-based luminosity signal. The two measurements differ by at most 1% throughout the whole data-taking period. Such a small variation was combined quadratically with the N_{MB} and σ_{MB} uncertainties, to get a total luminosity uncertainty of 3.8% for the p–Pb configuration (forward rapidities) and 3.5% for the Pb–p configuration (backward rapidities).

4 Results

The $\Upsilon(1S)$ production cross sections in p–Pb collisions at $\sqrt{s_{\text{NN}}} = 5.02$ TeV are:

$$\begin{aligned}\sigma_{\text{pPb}}^{\Upsilon(1S)}(-4.46 < y_{\text{cms}} < -2.96) &= 5.57 \pm 0.72(\text{stat}) \pm 0.60(\text{syst}) \mu\text{b}, \\ \sigma_{\text{pPb}}^{\Upsilon(1S)}(2.03 < y_{\text{cms}} < 3.53) &= 8.45 \pm 0.94(\text{stat}) \pm 0.77(\text{syst}) \mu\text{b}.\end{aligned}$$

The $\Upsilon(2S)$ production cross sections in p–Pb collisions at $\sqrt{s_{\text{NN}}} = 5.02$ TeV obtained in a similar way ($\text{BR}_{\Upsilon(2S) \rightarrow \mu^+ \mu^-} = 0.0193 \pm 0.0017$ [42]) are:

$$\begin{aligned}\sigma_{\text{pPb}}^{\Upsilon(2S)}(-4.46 < y_{\text{cms}} < -2.96) &= 1.85 \pm 0.61(\text{stat}) \pm 0.32(\text{syst}) \mu\text{b}, \\ \sigma_{\text{pPb}}^{\Upsilon(2S)}(2.03 < y_{\text{cms}} < 3.53) &= 2.97 \pm 0.82(\text{stat}) \pm 0.50(\text{syst}) \mu\text{b}.\end{aligned}$$

A summary of the different sources of systematic uncertainties and their relative value is given in Table 1².

Source	Backward rapidities	Forward rapidities
Signal extraction: $\Upsilon(1S)$	5%-6%(II)	4%-6%(II)
Signal extraction: $\Upsilon(2S)$	12%(II)	12%(II)
Input MC parameterization: $\Upsilon(1S)$	2%-5%(II)	4%-6%(II)
Input MC parameterization: $\Upsilon(2S)$	5%(II)	5%(II)
Tracking efficiency	6%(II)	4%(II)
Trigger efficiency	2%(II)	2%(II)
Matching efficiency	1%(II)	1%(II)
$\sigma_{\text{pp}}^{\Upsilon(1S)}$ (interpolation)	11%-13% (II)	7%-12%(II)
\mathcal{L} (correlated)	1.6%(I)	1.6%(I)
\mathcal{L} (uncorrelated)	3.1%(II)	3.4%(II)

Table 1: Summary of the relative systematic uncertainties on each quantity entering in the calculations of the results. Type I (II) stands for uncertainties correlated (uncorrelated) with rapidity. Type II uncertainties are given as a range including the smallest and the largest values observed in the bins considered in this analysis. Results are presented for the backward rapidity region ($-4.46 < y_{\text{cms}} < -2.96$), and for the forward rapidity one ($2.03 < y_{\text{cms}} < 3.53$).

The $\Upsilon(1S)$ candidates were further divided in four rapidity ranges, namely $-4.46 < y_{\text{cms}} < -3.53$, $-3.53 < y_{\text{cms}} < -2.96$, $2.03 < y_{\text{cms}} < 2.96$ and $2.96 < y_{\text{cms}} < 3.53$. Two of them are symmetric with respect to $y_{\text{cms}} = 0$. Figure 2 shows the inclusive $\Upsilon(1S)$ differential cross section $d\sigma/dy$ as a function of rapidity. The vertical error bars represent the statistical uncertainties and the open boxes the uncorrelated systematic uncertainties. Also shown is the inclusive $\Upsilon(1S)$ y -differential interpolated cross section in pp collisions at the same centre-of-mass energy (obtained as explained later in the text) scaled by A_{Pb} .

The CNM effects can be quantified with the nuclear modification factor,

$$R_{\text{pPb}}^{\Upsilon(1S)} = \frac{\sigma_{\text{pPb}}^{\Upsilon(1S)}}{A_{\text{Pb}} \times \sigma_{\text{pp}}^{\Upsilon(1S)}}, \quad (2)$$

²The uncertainties of type II are not fully uncorrelated with rapidity and no trivial factorization in correlated and uncorrelated parts can be made. Hence, they are labelled as uncorrelated, but they cannot be quadratically combined to obtain the rapidity integrated result.

where $\sigma_{\text{pp}}^{\Upsilon(1S)}$ is the $\Upsilon(1S)$ cross section in pp collisions at $\sqrt{s} = 5.02$ TeV.

Since $\sigma_{\text{pp}}^{\Upsilon(1S)}$ at $\sqrt{s} = 5.02$ TeV has not yet been measured, it was computed using a data driven \sqrt{s} interpolation method. A detailed description of the adopted procedure is given in [56]. The LHCb Collaboration has measured the $\Upsilon(1S)$ cross section in pp collisions at $\sqrt{s} = 2.76$ [52], 7 [45] and 8 [53] TeV, over the ranges $p_T < 15$ GeV/c and $2 < y < 4.5$, in 5 rapidity bins of equal size. The LHCb results were re-binned to obtain the cross section in (approximately) the rapidity ranges of interest for this analysis: $2 < y < 3$, $2 < y < 3.5$, $3 < y < 3.5$, $3 < y < 4.5$, and $3.5 < y < 4.5$. For each bin, the cross section as a function of energy was fitted according to 21 different shapes: 15 are based on Leading Order CEM (LO-CEM) calculations for Υ production, corresponding to various choices of PDFs and of the factorization scale; 3 are based on the energy-dependence of bare bottom-quark pair production (FONLL) [57]; the remaining three are a power law, a linear and an exponential function. The obtained fit parameters were used to compute the cross section at $\sqrt{s} = 5.02$ TeV. In order to take into account the rather poor agreement of the data with the fitting functions ($\chi^2/ndf > 2$ for all fits, where ndf is the number of degrees of freedom), all the uncertainties on the fit results were rescaled by $\sqrt{\chi^2/ndf}$. Fits with χ^2/ndf values larger than three times the minimum value obtained for the rapidity range considered were discarded. The weighted average of the surviving results was computed (using the rescaled fit uncertainty as a weight) and retained as central value. The average (rescaled) fit-result uncertainty was evaluated for each rapidity bin: it ranges from 7% to 12%. As an additional uncertainty, the maximum difference between the average and the individual fit results was computed: it ranges from 2% to 7%. Finally, a third uncertainty was considered, to take into account the shift of 0.035 rapidity units between the ranges adopted in the interpolation procedure and those used for the measurement of $R_{\text{pPb}}^{\Upsilon(1S)}$. Such an uncertainty is quantified by the maximum difference between the cross sections in the two ranges, evaluated with the LO-CEM and FONLL models, and amounts to 1% for the forward rapidity region and 3% for the backward rapidity region. Since the interpolation is performed separately for each rapidity range, the associated uncertainties are assumed to be uncorrelated with rapidity. For the forward and backward rapidity ranges used for the integrated results, the obtained interpolated cross-sections times branching ratio are 1451 ± 114 (syst) pb and 770 ± 87 (syst) pb, respectively.

Using the interpolated values of $\sigma_{\text{pp}}^{\Upsilon(1S)}$, the nuclear modification factors are

$$R_{\text{pPb}}^{\Upsilon(1S)}(-4.46 < y_{\text{cms}} < -2.96) = 0.86 \pm 0.11(\text{stat}) \pm 0.13(\text{uncorr}) \pm 0.01(\text{corr}),$$

$$R_{\text{pPb}}^{\Upsilon(1S)}(2.03 < y_{\text{cms}} < 3.53) = 0.70 \pm 0.08(\text{stat}) \pm 0.08(\text{uncorr}) \pm 0.01(\text{corr}).$$

Under the assumption of a $2 \rightarrow 1$ production process ($gg \rightarrow \Upsilon$), the sampled x_{Bj} are $5.5 \cdot 10^{-5} < x_{\text{Bj}} < 2.5 \cdot 10^{-4}$ and $3.6 \cdot 10^{-2} < x_{\text{Bj}} < 1.6 \cdot 10^{-1}$ at forward and backward rapidity, respectively. Thus, the measurement at forward rapidity tests the shadowing region and the one at backward rapidity the anti-shadowing region. In the case of a $2 \rightarrow 2$ production process ($gg \rightarrow \Upsilon g$) the covered x_{Bj} are naturally expected to be enlarged. In Fig. 3 the inclusive $\Upsilon(1S)$ nuclear modification factor in p–Pb collisions at $\sqrt{s_{\text{NN}}} = 5.02$ TeV is shown in four classes of rapidity. The vertical error bars represent the statistical uncertainties and the open boxes the uncorrelated systematic uncertainties. An additional correlated uncertainty is indicated by the full box around $R_{\text{pPb}} = 1$. The R_{pPb} shows a suppression of the inclusive $\Upsilon(1S)$ production yields at forward rapidity in p–Pb compared to pp collisions. At backward rapidity, the $\Upsilon(1S)$ R_{pPb} is compatible with unity within uncertainties, and therefore does not favour a strong gluon anti-shadowing. Also shown in Fig. 3 is the ALICE measurement of the inclusive $J/\psi R_{\text{pPb}}$ [32]. Although the uncertainties are large, it appears that at positive y_{cms} the $\Upsilon(1S)$ and $J/\psi R_{\text{pPb}}$ are rather similar. It is worth noting that due to its larger mass, the $\Upsilon(1S)$ R_{pPb} at forward rapidity is higher than the J/ψ one according to all available model calculations [25, 26, 28, 58]. At negative rapidities, the $J/\psi R_{\text{pPb}}$ are systematically above the $\Upsilon(1S)$ one but the two R_{pPb} are consistent within uncertainties.

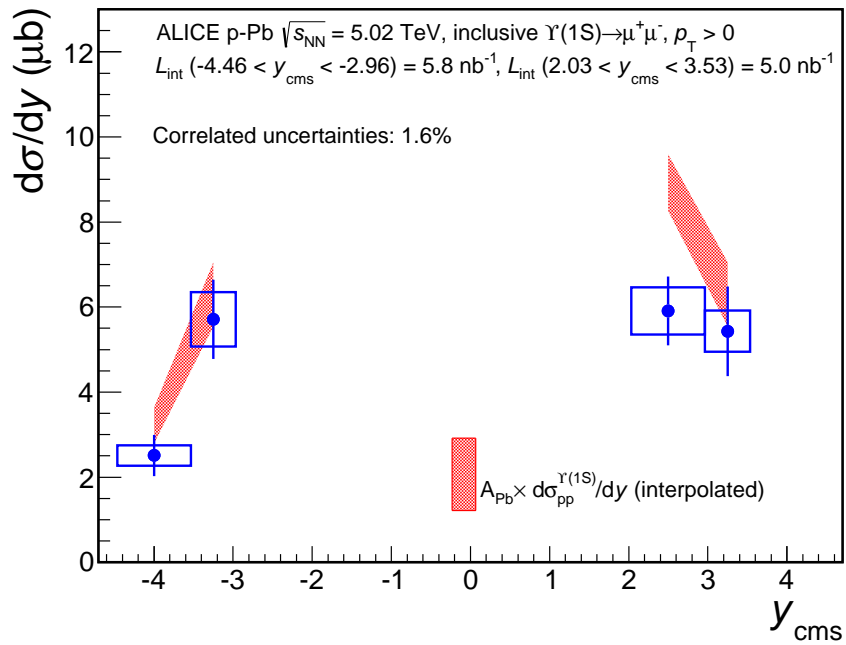


Fig. 2: Inclusive $\Upsilon(1S)$ production cross section as a function of rapidity in p–Pb collisions at $\sqrt{s_{NN}} = 5.02$ TeV. The vertical error bars represent the statistical uncertainties and the open boxes the uncorrelated systematic uncertainties. The correlated systematic uncertainty is directly quoted in the figure. It is obtained by summing in quadrature the correlated uncertainty on the integrated luminosity and the uncertainty on the branching ratio of $\Upsilon(1S)$ to dimuon. The bands correspond to the inclusive $\Upsilon(1S)$ pp cross section obtained with the procedure described in the text and scaled by A_{Pb} .

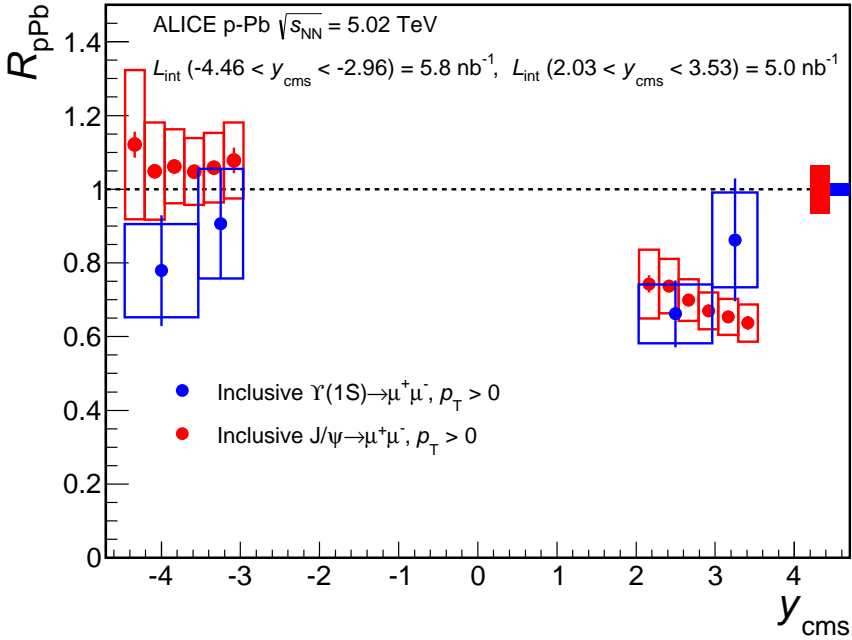


Fig. 3: Nuclear modification factor of inclusive $\Upsilon(1S)$ in p–Pb collisions at $\sqrt{s_{\text{NN}}} = 5.02$ TeV. The results are compared to those for inclusive J/ψ [32]. The vertical error bars represent the statistical uncertainties and the open boxes the uncorrelated systematic uncertainties (for the J/ψ , the uncorrelated and partially correlated uncertainties have been added in quadrature). The full boxes around $R_{\text{pPb}} = 1$ show the size of the correlated uncertainties, which in the case of the Υ include only the correlated uncertainty on the luminosity (see Tab. 1).

Although the rapidity ranges are not identical, the R_{pPb} measured by LHCb [59] are consistent with ALICE measurements within uncertainties, albeit systematically larger [56].

The ratio [$\Upsilon(2S)/\Upsilon(1S)$] of the production cross section of $\Upsilon(2S) \rightarrow \mu^+ \mu^-$ to $\Upsilon(1S) \rightarrow \mu^+ \mu^-$ can be obtained as

$$[\Upsilon(2S)/\Upsilon(1S)] = \frac{N[\Upsilon(2S)]/(A \times \epsilon)_{\Upsilon(1S)}}{N[\Upsilon(1S)]/(A \times \epsilon)_{\Upsilon(2S)}}. \quad (3)$$

The branching ratio of the dimuon decay channel does not enter the calculation. Additionally, since the same data sample is used \mathcal{L} cancels out in the ratio. The systematic uncertainties on the ratios were obtained by quadratically combining the systematic uncertainties entering in each element of Eq. 3. Nevertheless, since the decay kinematics of the two Υ states are close, the systematic uncertainties on tracking, trigger and matching efficiency, estimated for the same detector in the same working conditions, cancel out in the ratio. The results are:

$$[\Upsilon(2S)/\Upsilon(1S)]_{\text{pPb}}(-4.46 < y_{\text{cms}} < -2.96) = 0.26 \pm 0.09(\text{stat}) \pm 0.04(\text{syst}),$$

$$[\Upsilon(2S)/\Upsilon(1S)]_{\text{pPb}}(2.03 < y_{\text{cms}} < 3.53) = 0.27 \pm 0.08(\text{stat}) \pm 0.04(\text{syst}).$$

The same ratio has been measured by ALICE in pp collisions at $\sqrt{s} = 7$ TeV in the rapidity range $2.5 < y_{\text{cms}} < 4.0$ [60] and is $0.26 \pm 0.08(\text{tot})$, where the total (tot) uncertainty is the quadratic sum of the statistical and systematic uncertainties. The LHCb collaboration has measured the same ratio in pp collisions at $\sqrt{s} = 2.76, 7$ and 8 TeV and as a function of rapidity in the range $2.0 < y_{\text{cms}} < 4.5$ [45, 52, 53]. The measured $[\Upsilon(2S)/\Upsilon(1S)]$ is found to be, within uncertainties, independent of \sqrt{s} and rapidity. For $p_T < 15$ GeV/c (14 GeV/c for 8 TeV) the measured values in the range $3.0 < y_{\text{cms}} < 3.5$

are $0.22 \pm 0.03(\text{tot})$, $0.24 \pm 0.02(\text{tot})$ and $0.25 \pm 0.01(\text{tot})$ for $\sqrt{s} = 2.76$, 7 and 8 TeV, respectively. Our measured ratio [$\Upsilon(2S)/\Upsilon(1S)$] in p–Pb collisions is compatible with the same ratio in pp collisions. Within our uncertainties, there is therefore no evidence of a different magnitude of CNM effects for the $\Upsilon(2S)$ than for the $\Upsilon(1S)$. At mid-rapidity, however, the CMS collaboration has measured the double ratio, *i.e.* the ratio [$\Upsilon(2S)/\Upsilon(1S)$] in p–Pb divided by that in pp collisions, to be $0.83 \pm 0.05(\text{stat}) \pm 0.05(\text{syst})$, suggesting a stronger suppression of the $\Upsilon(2S)$ than of the $\Upsilon(1S)$ in p–Pb collisions [31].

The inclusive $\Upsilon(1S) R_{\text{pPb}}$ integrated over the backward or forward rapidity ranges, are compared to several model calculations in Fig. 4. In the left panel, the results are compared to a next-to-leading order (NLO) CEM calculation using the EPS09 parameterization of the nuclear modification of the gluon PDF (commonly referred to as gluon shadowing) at NLO [58] (blue shaded band) and to a parton energy loss calculation [25] with (green shaded band) or without (red band) EPS09 gluon shadowing at NLO. In the case of the CEM+EPS09 calculation, the band reflects the uncertainties of the calculation that are dominated by the ones of the EPS09 parameterization [19]. In the cases of the parton energy loss model calculations, the bands represent the uncertainty from the EPS09 parameterization or from the parton transport coefficient and the parameterization used for the pp reference cross section. None of the calculations fully describe the backward and forward rapidity data and all tend to overestimate the observed $\Upsilon(1S) R_{\text{pPb}}$. The parton energy loss with EPS09 calculation reproduces the $\Upsilon(1S) R_{\text{pPb}}$ at forward rapidity but tend to overestimate it at backward rapidity. The opposite trend is found for the parton energy loss calculation only.

In the right panel, the results are compared to a calculation of a $2 \rightarrow 2$ production model ($gg \rightarrow \Upsilon g$) at leading order (LO) using the EPS09 shadowing parameterization also at LO [28]. Two bands are shown to highlight the uncertainties linked to two different effects. The extent of the blue band shows the EPS09 LO related uncertainties in the shadowing region, *i.e.* at low x_{Bj} . The red band shows the uncertainty in the EMC region, *i.e.* at high x_{Bj} . As the authors of [28] discuss, the gluon nPDF is poorly known in this region and the $\Upsilon(1S) R_{\text{pPb}}$ at backward rapidity could add useful constraints to the model calculations. It is worth noting that the two blue bands in the left and right panels of Fig. 4 differ by their central curve and the extent of the uncertainties. The two approaches are similar and although the production models used are different, most of the difference comes from the usage of the NLO or LO EPS09 gluon shadowing parameterizations. It can be argued that using a NLO parameterization is more appropriate than a LO one, however it is worth remarking that other gluon shadowing parameterizations [20, 21] (also at NLO) are available and that the uncertainty band of the EPS09 LO parameterization practically includes them. Therefore, the blue uncertainty band in the right panel of Fig. 4 can be considered as including the uncertainty due to different gluon shadowing parameterizations. The backward rapidity $\Upsilon(1S) R_{\text{pPb}}$ disfavours the strong gluon anti-shadowing included in the EPS09 parameterization. In the right panel of Fig. 4, a calculation based on the CGC framework coupled with a CEM production model is also shown (green shaded band) for positive y_{cms} . It is worth noting that, although this calculation only slightly underestimates the $\Upsilon(1S) R_{\text{pPb}}$, it is not able to reproduce the $J/\psi R_{\text{pPb}}$ in the same rapidity range [32].

The quantity R_{FB} is defined as the ratio of the nuclear modification factors at forward and at backward rapidities in a range symmetric with respect to $y_{\text{cms}} = 0$. It can be computed directly from the ratio of the cross sections (see Eq. 1) of $\Upsilon(1S)$ at forward and backward rapidities. R_{FB} is therefore independent of $\sigma_{pp}^{\Upsilon(1S)}$. The drawback of the R_{FB} ratio is that it can only be measured in the restricted rapidity range $2.96 < |y_{\text{cms}}| < 3.53$, hence losing about two thirds of the number of measured Υ . The measured forward to backward ratio is $R_{\text{FB}}(2.96 < |y_{\text{cms}}| < 3.53) = 0.95 \pm 0.24(\text{stat}) \pm 0.14(\text{syst})$. Uncertainties are obtained by summing in quadrature the contribution of each individual element entering the ratio. The inclusive $\Upsilon(1S) R_{\text{FB}}$ is compared in Fig. 5 to the inclusive $J/\psi R_{\text{FB}}$ [32] in the same rapidity range (left panel) and to several model calculations (right panel). In the rapidity range $2.96 < |y_{\text{cms}}| < 3.53$ the $\Upsilon(1S) R_{\text{FB}}$ is compatible with unity and is larger than that of the J/ψ . All models describe the data within

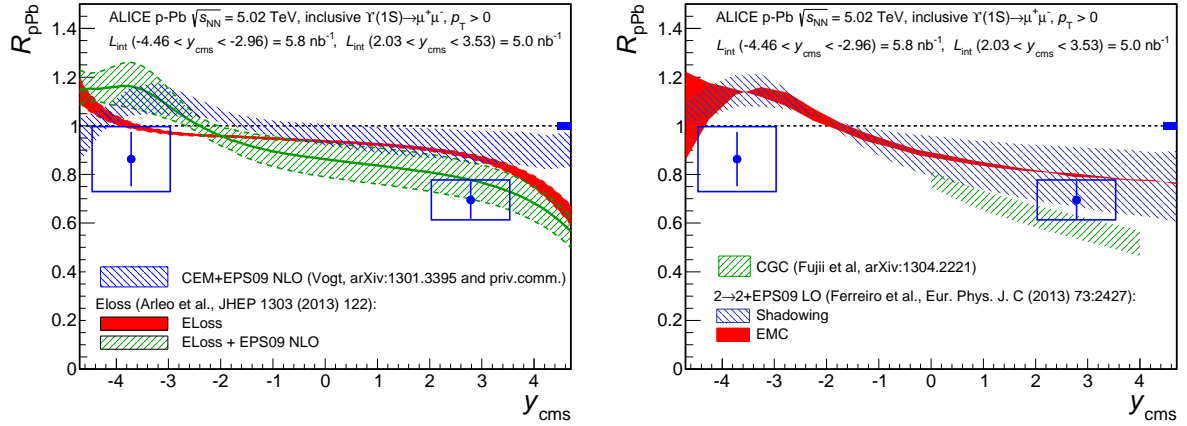


Fig. 4: Nuclear modification factor of inclusive $\Upsilon(1S)$ in p–Pb collisions at $\sqrt{s_{NN}} = 5.02$ TeV as a function of rapidity. The vertical error bars represent the statistical uncertainties and the open boxes the uncorrelated systematic uncertainties. The full boxes around $R_{p\text{Pb}} = 1$ show the size of the correlated uncertainties. Also shown are several model calculations: (left) parton energy loss [25] with and without EPS09 shadowing at NLO and CEM with EPS09 shadowing at NLO [58]; (right) CGC based [26] and CSM with EPS09 shadowing at LO [28]. For the latter the effect of variation in the shadowing and EMC curves is highlighted as described in the text.

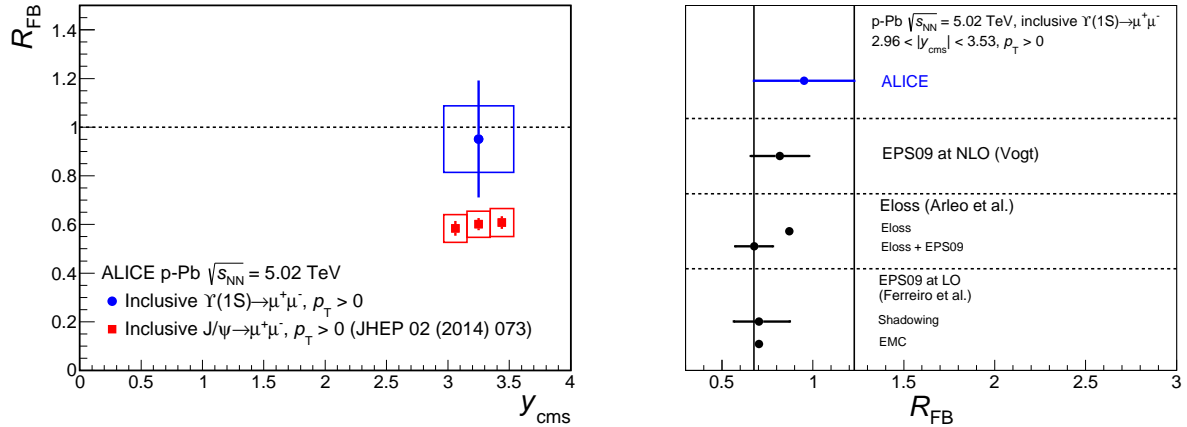


Fig. 5: (Left) Forward to backward ratio R_{FB} of inclusive $\Upsilon(1S)$ yields compared to the $J/\psi R_{FB}$ [32]. The vertical error bars represent the statistical uncertainties and the open boxes the uncorrelated systematic uncertainties. (Right) Inclusive $\Upsilon(1S) R_{FB}$ compared to theoretical model calculations. The statistical and systematic uncertainties for the experimental value are added in quadrature. For the calculations, uncertainties are quoted when available.

the present uncertainties of the measurement.

5 Conclusion

In summary, we reported the ALICE measurement of Υ production in p–Pb collisions at $\sqrt{s_{NN}} = 5.02$ TeV at the LHC. The $\Upsilon(1S)$ production cross section and nuclear modification factor were presented in the rapidity ranges $-4.46 < y_{\text{cms}} < -2.96$ and $2.03 < y_{\text{cms}} < 3.53$ down to zero transverse momentum. At forward rapidity, $R_{p\text{Pb}}$ shows a suppression of $\Upsilon(1S)$ production in p–Pb compared to pp collisions. At backward rapidity, the $\Upsilon(1S) R_{p\text{Pb}}$ is consistent with unity, suggesting a small gluon anti-shadowing. Models including the nuclear modification of the gluon PDF [28, 58] or a contribution from coherent parton energy loss [25] tend to overestimate our measured $R_{p\text{Pb}}$ and cannot simultaneously describe the forward and backward rapidity suppressions. A CGC based model [26] is in agreement with our

Υ results at forward rapidity but cannot describe the $J/\psi R_{\text{pPb}}$ [32]. The forward to backward ratio R_{FB} of the inclusive $\Upsilon(1S)$ yields in $2.96 < |y_{\text{cms}}| < 3.53$ is compatible with unity within large uncertainties. Within our uncertainties, the [$\Upsilon(2S)/\Upsilon(1S)$] ratio shows no evidence of different CNM effects on the two states. Additional measurements with higher statistics are needed to further constrain the models and extrapolate the CNM effects to Pb–Pb collisions.

Acknowledgements

The ALICE Collaboration would like to thank all its engineers and technicians for their invaluable contributions to the construction of the experiment and the CERN accelerator teams for the outstanding performance of the LHC complex.

The ALICE Collaboration gratefully acknowledges the resources and support provided by all Grid centres and the Worldwide LHC Computing Grid (WLCG) collaboration.

The ALICE Collaboration acknowledges the following funding agencies for their support in building and running the ALICE detector:

State Committee of Science, World Federation of Scientists (WFS) and Swiss Fonds Kidagan, Armenia, Conselho Nacional de Desenvolvimento Científico e Tecnológico (CNPq), Financiadora de Estudos e Projetos (FINEP), Fundação de Amparo à Pesquisa do Estado de São Paulo (FAPESP);

National Natural Science Foundation of China (NSFC), the Chinese Ministry of Education (CMOE) and the Ministry of Science and Technology of China (MSTC);

Ministry of Education and Youth of the Czech Republic;

Danish Natural Science Research Council, the Carlsberg Foundation and the Danish National Research Foundation;

The European Research Council under the European Community's Seventh Framework Programme;

Helsinki Institute of Physics and the Academy of Finland;

French CNRS-IN2P3, the ‘Region Pays de Loire’, ‘Region Alsace’, ‘Region Auvergne’ and CEA, France;

German BMBF and the Helmholtz Association;

General Secretariat for Research and Technology, Ministry of Development, Greece;

Hungarian OTKA and National Office for Research and Technology (NKTH);

Department of Atomic Energy and Department of Science and Technology of the Government of India;

Istituto Nazionale di Fisica Nucleare (INFN) and Centro Fermi - Museo Storico della Fisica e Centro Studi e Ricerche ”Enrico Fermi”, Italy;

MEXT Grant-in-Aid for Specially Promoted Research, Japan;

Joint Institute for Nuclear Research, Dubna;

National Research Foundation of Korea (NRF);

CONACYT, DGAPA, México, ALFA-EC and the EPLANET Program (European Particle Physics Latin American Network)

Stichting voor Fundamenteel Onderzoek der Materie (FOM) and the Nederlandse Organisatie voor Wetenschappelijk Onderzoek (NWO), Netherlands;

Research Council of Norway (NFR);

Polish Ministry of Science and Higher Education;

National Science Centre, Poland;

Ministry of National Education/Institute for Atomic Physics and CNCS-UEFISCDI - Romania;

Ministry of Education and Science of Russian Federation, Russian Academy of Sciences, Russian Federal Agency of Atomic Energy, Russian Federal Agency for Science and Innovations and The Russian Foundation for Basic Research;

Ministry of Education of Slovakia;

Department of Science and Technology, South Africa;

CIEMAT, EELA, Ministerio de Economía y Competitividad (MINECO) of Spain, Xunta de Galicia

(Consellería de Educación), CEADEN, Cubaenergía, Cuba, and IAEA (International Atomic Energy Agency);
 Swedish Research Council (VR) and Knut & Alice Wallenberg Foundation (KAW);
 Ukraine Ministry of Education and Science;
 United Kingdom Science and Technology Facilities Council (STFC);
 The United States Department of Energy, the United States National Science Foundation, the State of Texas, and the State of Ohio;
 Ministry of Science, Education and Sports of Croatia and Unity through Knowledge Fund, Croatia.

References

- [1] N. Brambilla, S. Eidelman, B. Heltsley, R. Vogt, G. Bodwin, et al., Heavy quarkonium: progress, puzzles, and opportunities, *Eur. Phys. J.* C71 (2011) 1534. [arXiv:1010.5827](https://arxiv.org/abs/1010.5827), doi:[10.1140/epjc/s10052-010-1534-9](https://doi.org/10.1140/epjc/s10052-010-1534-9).
- [2] H. Fritzsch, Producing Heavy Quark Flavors in Hadronic Collisions: A Test of Quantum Chromodynamics, *Phys. Lett.* B67 (1977) 217. doi:[10.1016/0370-2693\(77\)90108-3](https://doi.org/10.1016/0370-2693(77)90108-3).
- [3] J. Amundson, O. J. Eboli, E. Gregores, F. Halzen, Quantitative tests of color evaporation: Charmonium production, *Phys. Lett.* B390 (1997) 323–328. [arXiv:hep-ph/9605295](https://arxiv.org/abs/hep-ph/9605295), doi:[10.1016/S0370-2693\(96\)01417-7](https://doi.org/10.1016/S0370-2693(96)01417-7).
- [4] R. Baier, R. Ruckl, Hadronic Production of J/ψ and Υ : Transverse Momentum Distributions, *Phys. Lett.* B102 (1981) 364. doi:[10.1016/0370-2693\(81\)90636-5](https://doi.org/10.1016/0370-2693(81)90636-5).
- [5] G. T. Bodwin, E. Braaten, G. P. Lepage, Rigorous QCD analysis of inclusive annihilation and production of heavy quarkonium, *Phys. Rev.* D51 (1995) 1125–1171. [arXiv:hep-ph/9407339](https://arxiv.org/abs/hep-ph/9407339), doi:[10.1103/PhysRevD.55.5853](https://doi.org/10.1103/PhysRevD.55.5853), [10.1103/PhysRevD.51.1125](https://doi.org/10.1103/PhysRevD.51.1125).
- [6] J. Lansberg, J/ψ , ψ' and Υ production at hadron colliders: A Review, *Int. J. Mod. Phys.* A21 (2006) 3857–3916. [arXiv:hep-ph/0602091](https://arxiv.org/abs/hep-ph/0602091), doi:[10.1142/S0217751X06033180](https://doi.org/10.1142/S0217751X06033180).
- [7] J. C. Collins, M. Perry, Superdense Matter: Neutrons Or Asymptotically Free Quarks?, *Phys.Rev.Lett.* 34 (1975) 1353. doi:[10.1103/PhysRevLett.34.1353](https://doi.org/10.1103/PhysRevLett.34.1353).
- [8] E. V. Shuryak, Quantum Chromodynamics and the Theory of Superdense Matter, *Phys.Rept.* 61 (1980) 71–158. doi:[10.1016/0370-1573\(80\)90105-2](https://doi.org/10.1016/0370-1573(80)90105-2).
- [9] T. Matsui, H. Satz, J/ψ Suppression by Quark-Gluon Plasma Formation, *Phys. Lett.* B178 (1986) 416. doi:[10.1016/0370-2693\(86\)91404-8](https://doi.org/10.1016/0370-2693(86)91404-8).
- [10] S. Chatrchyan, et al., Observation of sequential Upsilon suppression in PbPb collisions, *Phys. Rev. Lett.* 109 (2012) 222301. [arXiv:1208.2826](https://arxiv.org/abs/1208.2826), doi:[10.1103/PhysRevLett.109.222301](https://doi.org/10.1103/PhysRevLett.109.222301).
- [11] S. Chatrchyan, et al., Indications of suppression of excited Υ states in PbPb collisions at $\sqrt{s_{NN}} = 2.76$ TeV, *Phys. Rev. Lett.* 107 (2011) 052302. [arXiv:1105.4894](https://arxiv.org/abs/1105.4894), doi:[10.1103/PhysRevLett.107.052302](https://doi.org/10.1103/PhysRevLett.107.052302).
- [12] B. Abelev, et al., J/ψ Suppression at Forward Rapidity in Pb-Pb Collisions at $\sqrt{s_{NN}} = 2.76$ TeV, *Phys. Rev. Lett.* 109 (7) (2012) 072301. [arXiv:1202.1383](https://arxiv.org/abs/1202.1383), doi:[10.1103/PhysRevLett.109.072301](https://doi.org/10.1103/PhysRevLett.109.072301).
- [13] E. Abbas, et al., J/ψ Elliptic Flow in Pb-Pb Collisions at $\sqrt{s_{NN}} = 2.76$ TeV, *Phys. Rev. Lett.* 111 (16) (2013) 162301. [arXiv:1303.5880](https://arxiv.org/abs/1303.5880), doi:[10.1103/PhysRevLett.111.162301](https://doi.org/10.1103/PhysRevLett.111.162301).

- [14] B. B. Abelev, et al., Centrality, rapidity and transverse momentum dependence of J/Ψ suppression in Pb-Pb collisions at $\sqrt{s_{NN}}=2.76$ TeV, Phys.Lett. B743 (2014) 314–327. arXiv:1311.0214, doi:10.1016/j.physletb.2014.05.064.
- [15] R. L. Thews, M. Schroedter, J. Rafelski, Enhanced J/ψ production in deconfined quark matter, Phys. Rev. C63 (2001) 054905. arXiv:hep-ph/0007323, doi:10.1103/PhysRevC.63.054905.
- [16] L. Grandchamp, R. Rapp, Thermal versus direct J/ψ production in ultrarelativistic heavy ion collisions, Phys.Lett. B523 (2001) 60–66. arXiv:hep-ph/0103124, doi:10.1016/S0370-2693(01)01311-9.
- [17] P. Braun-Munzinger, J. Stachel, (Non)thermal aspects of charmonium production and a new look at J/ψ suppression, Phys. Lett. B490 (2000) 196–202. doi:10.1016/S0370-2693(00)00991-6.
- [18] A. Emerick, X. Zhao, R. Rapp, Bottomonia in the Quark-Gluon Plasma and their Production at RHIC and LHC, Eur.Phys.J. A48 (2012) 72. arXiv:1111.6537, doi:10.1140/epja/i2012-12072-y.
- [19] K. Eskola, H. Paukkunen, C. Salgado, EPS09: A New Generation of NLO and LO Nuclear Parton Distribution Functions, JHEP 0904 (2009) 065. arXiv:0902.4154, doi:10.1088/1126-6708/2009/04/065.
- [20] D. de Florian, R. Sassot, Nuclear parton distributions at next-to-leading order, Phys. Rev. D69 (2004) 074028. arXiv:hep-ph/0311227, doi:10.1103/PhysRevD.69.074028.
- [21] D. de Florian, R. Sassot, P. Zurita, M. Stratmann, Global Analysis of Nuclear Parton Distributions, Phys. Rev. D85 (2012) 074028. arXiv:1112.6324, doi:10.1103/PhysRevD.85.074028.
- [22] M. Hirai, S. Kumano, T.-H. Nagai, Determination of nuclear parton distribution functions and their uncertainties in next-to-leading order, Phys.Rev. C76 (2007) 065207. arXiv:0709.3038, doi:10.1103/PhysRevC.76.065207.
- [23] S. Gavin, J. Milana, Energy loss at large $x(F)$ in nuclear collisions, Phys.Rev.Lett. 68 (1992) 1834–1837. doi:10.1103/PhysRevLett.68.1834.
- [24] S. J. Brodsky, P. Hoyer, A Bound on the energy loss of partons in nuclei, Phys.Lett. B298 (1993) 165–170. arXiv:hep-ph/9210262, doi:10.1016/0370-2693(93)91724-2.
- [25] F. Arleo, S. Peigne, Heavy-quarkonium suppression in p-A collisions from parton energy loss in cold QCD matter, JHEP 1303 (2013) 122. arXiv:1212.0434, doi:10.1007/JHEP03(2013)122.
- [26] H. Fujii, K. Watanabe, Heavy quark pair production in high energy pA collisions: Quarkonium, Nucl. Phys. A915 (2013) 1–23. arXiv:1304.2221, doi:10.1016/j.nuclphysa.2013.06.011.
- [27] R. Vogt, Cold Nuclear Matter Effects on J/ψ and Υ Production at the LHC, Phys.Rev. C81 (2010) 044903. arXiv:1003.3497, doi:10.1103/PhysRevC.81.044903.
- [28] E. Ferreiro, F. Fleuret, J. Lansberg, N. Matagne, A. Rakotozafindrabe, Υ production in p(d)A collisions at RHIC and the LHC, Eur. Phys. J. C73 (2011) 2427. arXiv:1110.5047, doi:10.1140/epjc/s10052-013-2427-5.

- [29] A. Adare, et al., $\Upsilon(1S + 2S + 3S)$ production in $d+\text{Au}$ and $p+p$ collisions at $\sqrt{s_{NN}} = 200$ GeV and cold-nuclear matter effects, Phys. Rev. C87 (2013) 044909. arXiv:1211.4017, doi:10.1103/PhysRevC.87.044909.
- [30] L. Adamczyk, et al., Suppression of Υ Production in $d+\text{Au}$ and $\text{Au}+\text{Au}$ Collisions at $\sqrt{s_{NN}} = 200$ GeV, Phys.Lett. B735 (2014) 127. arXiv:1312.3675, doi:10.1016/j.physletb.2014.06.028.
- [31] S. Chatrchyan, et al., Event activity dependence of $\Upsilon(nS)$ production in $\sqrt{s_{NN}}=5.02$ TeV $p\text{Pb}$ and $\sqrt{s}=2.76$ TeV pp collisions, JHEP 04 (2014) 103. arXiv:1312.6300, doi:10.1007/JHEP04(2014)103.
- [32] B. B. Abelev, et al., J/ψ production and nuclear effects in $p\text{-Pb}$ collisions at $\sqrt{s_{NN}} = 5.02$ TeV, JHEP 1402 (2014) 073. arXiv:1308.6726, doi:10.1007/JHEP02(2014)073.
- [33] R. Aaij, et al., Study of J/ψ production and cold nuclear matter effects in $p\text{Pb}$ collisions at $\sqrt{s_{NN}} = 5$ TeV, JHEP 1402 (2014) 072. arXiv:1308.6729, doi:10.1007/JHEP02(2014)072.
- [34] B. B. Abelev, et al., Suppression of $\Upsilon(1S)$ at forward rapidity in Pb-Pb collisions at $\sqrt{s_{NN}} = 2.76$ TeV, arXiv:1405.4493.
- [35] K. Aamodt, et al., The ALICE experiment at the CERN LHC, JINST 3 (2008) S08002. doi:10.1088/1748-0221/3/08/S08002.
- [36] B. B. Abelev, et al., Performance of the ALICE Experiment at the CERN LHC, arXiv:1402.4476.
- [37] F. Bossu, M. Gagliardi, M. Marchisone, Performance of the RPC-based ALICE muon trigger system at the LHC, JINST 7 (2012) T12002. arXiv:1211.1948, doi:10.1088/1748-0221/7/12/T12002.
- [38] K. Aamodt, et al., Alignment of the ALICE Inner Tracking System with cosmic-ray tracks, JINST 5 (2010) P03003. arXiv:1001.0502, doi:10.1088/1748-0221/5/03/P03003.
- [39] E. Abbas, et al., Performance of the ALICE VZERO system, JINST 8 (2013) P10016. arXiv:1306.3130, doi:10.1088/1748-0221/8/10/P10016.
- [40] K. Aamodt, et al., Rapidity and transverse momentum dependence of inclusive J/ψ production in pp collisions at $\sqrt{s} = 7$ TeV, Phys. Lett. B704 (2011) 442–455. arXiv:1105.0380, doi:10.1016/j.physletb.2011.09.054, 10.1016/j.physletb.2012.10.060.
- [41] J. Gaiser, SLAC Stanford - SLAC-255 (82.REC.JUN.83) 194, <http://www/slac.stanford.edu/cgi-wrap/getdoc/slac-r-255.pdf>.
- [42] J. Beringer, et al., Review of Particle Physics (RPP), Phys. Rev. D86 (2012) 010001. doi:10.1103/PhysRevD.86.010001.
- [43] F. Bossu, Z. C. del Valle, A. de Falco, M. Gagliardi, S. Grigoryan, et al., Phenomenological interpolation of the inclusive J/ψ cross section to proton-proton collisions at 2.76 TeV and 5.5 TeV, arXiv:1103.2394.
- [44] D. Acosta, et al., Υ production and polarization in $p\bar{p}$ collisions at $\sqrt{s} = 1.8$ -TeV, Phys. Rev. Lett. 88 (2002) 161802. doi:10.1103/PhysRevLett.88.161802.
- [45] R. Aaij, et al., Measurement of Υ production in pp collisions at $\sqrt{s} = 7$ TeV, Eur. Phys. J. C72 (2012) 2025. arXiv:1202.6579, doi:10.1140/epjc/s10052-012-2025-y.

- [46] V. Khachatryan, et al., Measurement of the Inclusive Υ production cross section in $p\bar{p}$ collisions at $\sqrt{s} = 7$ TeV, Phys. Rev. D83 (2011) 112004. arXiv:1012.5545, doi:10.1103/PhysRevD.83.112004.
- [47] K. Eskola, V. Kolhinen, C. Salgado, The Scale dependent nuclear effects in parton distributions for practical applications, Eur. Phys. J. C9 (1999) 61–68. arXiv:hep-ph/9807297, doi:10.1007/s100520050513.
- [48] V. Abazov, et al., Measurement of the polarization of the Υ_{1S} and Υ_{2S} states in $p\bar{p}$ collisions at $\sqrt{s} = 1.96$ -TeV, Phys. Rev. Lett. 101 (2008) 182004. arXiv:0804.2799, doi:10.1103/PhysRevLett.101.182004.
- [49] J. S. Russ, Polarization in Quarkonium Production, arXiv:1208.4292.
- [50] S. Chatrchyan, et al., Measurement of the $\Upsilon(1S)$, $\Upsilon(2S)$ and $\Upsilon(3S)$ polarizations in $p\bar{p}$ collisions at $\sqrt{s} = 7$ TeV, Phys. Rev. Lett. 110 (2013) 081802. arXiv:1209.2922, doi:10.1103/PhysRevLett.110.081802.
- [51] R. Brun, F. Carminati, S. Giani, GEANT Detector Description and Simulation Tool, CERN Program Library Long Writeup CERN-W5013.
- [52] R. Aaij, et al., Measurement of Υ production in $p\bar{p}$ collisions at $\sqrt{s} = 2.76$ TeV, Eur. Phys. J. C74 (2014) 2835. arXiv:1402.2539, doi:10.1140/epjc/s10052-014-2835-1.
- [53] R. Aaij, et al., Production of J/ψ and Υ mesons in $p\bar{p}$ collisions at $\sqrt{s} = 8$ TeV, JHEP 1306 (2013) 064. arXiv:1304.6977, doi:10.1007/JHEP06(2013)064.
- [54] S. van der Meer, Calibration of the effective beam height in the ISR, CERN-ISR-PO-68-31. <http://cds.cern.ch/record/296752>.
- [55] B. Abelev, et al., Measurement of visible cross sections in proton-lead collisions at $\sqrt{s_{NN}} = 5.02$ TeV in van der Meer scans with the ALICE detector, arXiv:1405.1849.
- [56] ALICE Collaboration and LHCb Collaboration, Reference pp cross-sections for (1S) studies in proton-lead collisions at $s_{NN} = 5.02$ TeV and comparisons between ALICE and LHCb results, ALICE-PUBLIC-2014-002, LHCb-CONF-2014-003.
- [57] M. Cacciari, et al., Theoretical predictions for charm and bottom production at the LHC, JHEP 1210 (2012) 137. arXiv:1205.6344.
- [58] J. Albacete, N. Armesto, R. Baier, G. Barnafoldi, J. Barrette, et al., Predictions for $p+\text{Pb}$ Collisions at $\sqrt{s_{NN}} = 5$ TeV, Int. J. Mod. Phys. E22 (2013) 1330007. arXiv:1301.3395, doi:10.1142/S0218301313300075.
- [59] R. Aaij, et al., Study of Υ production and cold nuclear matter effects in $p\text{Pb}$ collisions at $\sqrt{s_{NN}} = 5$ TeV, JHEP 1407 (2014) 094. arXiv:1405.5152, doi:10.1007/JHEP07(2014)094.
- [60] B. B. Abelev, et al., Measurement of quarkonium production at forward rapidity in $p\bar{p}$ collisions at $\sqrt{s} = 7$ TeV, Eur. Phys. J. C74 (2014) 2974. arXiv:1403.3648, doi:10.1140/epjc/s10052-014-2974-4.

A The ALICE Collaboration

- B. Abelev⁷², J. Adam³⁸, D. Adamová⁸⁰, M.M. Aggarwal⁸⁴, G. Aglieri Rinella³⁵, M. Agnello^{108,91}, A. Agostinelli²⁷, N. Agrawal⁴⁵, Z. Ahammed¹²⁸, N. Ahmad¹⁸, I. Ahmed¹⁵, S.U. Ahn⁶⁵, S.A. Ahn⁶⁵, I. Aimo^{91,108}, S. Aiola¹³³, M. Ajaz¹⁵, A. Akindinov⁵⁵, S.N. Alam¹²⁸, D. Aleksandrov⁹⁷, B. Alessandro¹⁰⁸, D. Alexandre⁹⁹, A. Alici^{102,12}, A. Alkin³, J. Alme³⁶, T. Alt⁴⁰, S. Altinpinar¹⁷, I. Altsybeev¹²⁷, C. Alves Garcia Prado¹¹⁶, C. Andrei⁷⁵, A. Andronic⁹⁴, V. Anguelov⁹⁰, J. Anielski⁵¹, T. Antićic⁹⁵, F. Antinori¹⁰⁵, P. Antonioli¹⁰², L. Aphecetche¹¹⁰, H. Appelshäuser⁵⁰, S. Arcelli²⁷, N. Armesto¹⁶, R. Arnaldi¹⁰⁸, T. Aronsson¹³³, I.C. Arsene^{94,21}, M. Arslanbekov⁵⁰, A. Augustinus³⁵, R. Averbeck⁹⁴, T.C. Awes⁸¹, M.D. Azmi^{86,18}, M. Bach⁴⁰, A. Badalà¹⁰⁴, Y.W. Baek^{67,41}, S. Bagnasco¹⁰⁸, R. Bailhache⁵⁰, R. Bala⁸⁷, A. Baldissari¹⁴, F. Baltasar Dos Santos Pedrosa³⁵, R.C. Baral⁵⁸, R. Barbera²⁸, F. Barile³², G.G. Barnaföldi¹³², L.S. Barnby⁹⁹, V. Barret⁶⁷, J. Bartke¹¹³, E. Bartsch⁵⁰, M. Basile²⁷, N. Bastid⁶⁷, S. Basu¹²⁸, B. Bathen⁵¹, G. Batigne¹¹⁰, A. Batista Camejo⁶⁷, B. Batyunya⁶³, P.C. Batzing²¹, C. Baumann⁵⁰, I.G. Bearden⁷⁷, H. Beck⁵⁰, C. Bedda⁹¹, N.K. Behera⁴⁵, I. Belikov⁵², F. Bellini²⁷, R. Bellwied¹¹⁸, R. Belmont¹³¹, E. Belmont-Moreno⁶¹, V. Belyaev⁷³, G. Bencedi¹³², S. Beole²⁶, I. Berceanu⁷⁵, A. Bercuci⁷⁵, Y. Berdnikov^{ii,82}, D. Berenyi¹³², R.A. Bertens⁵⁴, D. Berzana²⁶, L. Betev³⁵, A. Bhasin⁸⁷, I.R. Bhat⁸⁷, A.K. Bhati⁸⁴, B. Bhattacharjee⁴², J. Bhom¹²⁴, L. Bianchi²⁶, N. Bianchi⁶⁹, C. Bianchin⁵⁴, J. Bielčík³⁸, J. Bielčíková⁸⁰, A. Bilandžić⁷⁷, S. Bjelogrlic⁵⁴, F. Blanco¹⁰, D. Blau⁹⁷, C. Blume⁵⁰, F. Bock^{90,71}, A. Bogdanov⁷³, H. Bøggild⁷⁷, M. Bogolyubsky¹⁰⁹, F.V. Böhmer⁸⁹, L. Boldizsár¹³², M. Bombara³⁹, J. Book⁵⁰, H. Borel¹⁴, A. Borissov^{93,131}, M. Borri⁷⁹, F. Bossú⁶², M. Botje⁷⁸, E. Botta²⁶, S. Böttger⁴⁹, P. Braun-Munzinger⁹⁴, M. Bregant¹¹⁶, T. Breitner⁴⁹, T.A. Broker⁵⁰, T.A. Browning⁹², M. Broz³⁸, E. Bruna¹⁰⁸, G.E. Bruno³², D. Budnikov⁹⁶, H. Buesching⁵⁰, S. Bufalino¹⁰⁸, P. Buncic³⁵, O. Busch⁹⁰, Z. Buthelezi⁶², D. Caffarri^{35,29}, X. Cai⁷, H. Caines¹³³, A. Caliva⁵⁴, E. Calvo Villar¹⁰⁰, P. Camerini²⁵, F. Carena³⁵, W. Carena³⁵, J. Castillo Castellanos¹⁴, A.J. Castro¹²¹, E.A.R. Casula²⁴, V. Catanescu⁷⁵, C. Cavicchioli³⁵, C. Ceballos Sanchez⁹, J. Cepila³⁸, P. Cerello¹⁰⁸, B. Chang¹¹⁹, S. Chapelard³⁵, J.L. Charvet¹⁴, S. Chattopadhyay¹²⁸, S. Chattopadhyay⁹⁸, V. Chelnokov³, M. Cherney⁸³, C. Cheshkov¹²⁶, B. Cheynis¹²⁶, V. Chibante Barroso³⁵, D.D. Chinellato¹¹⁷, P. Chochula³⁵, M. Chojnacki⁷⁷, S. Choudhury¹²⁸, P. Christakoglou⁷⁸, C.H. Christensen⁷⁷, P. Christiansen³³, T. Chujo¹²⁴, S.U. Chung⁹³, C. Cicalo¹⁰³, L. Cifarelli^{12,27}, F. Cindolo¹⁰², J. Cleymans⁸⁶, F. Colamaria³², D. Colella³², A. Collu²⁴, M. Colocci²⁷, G. Conesa Balbastre⁶⁸, Z. Conesa del Valle⁴⁸, M.E. Connors¹³³, J.G. Contreras^{11,38}, T.M. Cormier^{81,131}, Y. Corrales Morales²⁶, P. Cortese³¹, I. Cortés Maldonado², M.R. Cosentino¹¹⁶, F. Costa³⁵, P. Crochet⁶⁷, R. Cruz Albino¹¹, E. Cuautle⁶⁰, L. Cunqueiro³⁵, A. Dainese¹⁰⁵, R. Dang⁷, A. Danu⁵⁹, D. Das⁹⁸, I. Das⁴⁸, K. Das⁹⁸, S. Das⁴, A. Dash¹¹⁷, S. Dash⁴⁵, S. De¹²⁸, H. Delagrange^{110,ii}, A. Deloff⁷⁴, E. Dénes¹³², G. D'Erasmo³², A. De Caro^{30,12}, G. de Cataldo¹⁰¹, J. de Cuveland⁴⁰, A. De Falco²⁴, D. De Gruttola^{12,30}, N. De Marco¹⁰⁸, S. De Pasquale³⁰, R. de Rooij⁵⁴, M.A. Diaz Corchero¹⁰, T. Dietel^{86,51}, P. Dillenseger⁵⁰, R. Divià³⁵, D. Di Bari³², S. Di Liberto¹⁰⁶, A. Di Mauro³⁵, P. Di Nezza⁶⁹, Ø. Djupsland¹⁷, A. Dobrin⁵⁴, T. Dobrowolski⁷⁴, D. Domenicis Giménez¹¹⁶, B. Dönigus⁵⁰, O. Dordic²¹, S. Dörheim⁸⁹, A.K. Dubey¹²⁸, A. Dubla⁵⁴, L. Ducroux¹²⁶, P. Dupieux⁶⁷, A.K. Dutta Majumdar⁹⁸, T. E. Hilden⁴³, R.J. Ehlers¹³³, D. Elia¹⁰¹, H. Engel⁴⁹, B. Erazmus^{110,35}, H.A. Erdal³⁶, D. Eschweiler⁴⁰, B. Espagnon⁴⁸, M. Esposito³⁵, M. Estienne¹¹⁰, S. Esumi¹²⁴, D. Evans⁹⁹, S. Evdokimov¹⁰⁹, D. Fabris¹⁰⁵, J. Faivre⁶⁸, D. Falchieri²⁷, A. Fantoni⁶⁹, M. Fasel^{90,71}, D. Fehlker¹⁷, L. Feldkamp⁵¹, D. Feleá⁵⁹, A. Feliciello¹⁰⁸, G. Feofilov¹²⁷, J. Ferencei⁸⁰, A. Fernández Téllez², E.G. Ferreiro¹⁶, A. Ferretti²⁶, A. Festanti²⁹, J. Figiel¹¹³, M.A.S. Figueredo¹²⁰, S. Filchagin⁹⁶, D. Finogeev⁵³, F.M. Fianda¹⁰¹, E.M. Fiore³², E. Floratos⁸⁵, M. Floris³⁵, S. Foertsch⁶², P. Foka⁹⁴, S. Fokin⁹⁷, E. Fragiacomo¹⁰⁷, A. Francescon^{29,35}, U. Frankenfeld⁹⁴, U. Fuchs³⁵, C. Furget⁶⁸, A. Furs⁵³, M. Fusco Girardi³⁰, J.J. Gaardhøje⁷⁷, M. Gagliardi²⁶, A.M. Gago¹⁰⁰, M. Gallio²⁶, D.R. Gangadharan^{71,19}, P. Ganoti^{81,85}, C. Gao⁷, C. Garabatos⁹⁴, E. Garcia-Solis¹³, C. Gargiulo³⁵, I. Garishvili⁷², M. Germain¹¹⁰, A. Gheata³⁵, M. Gheata^{35,59}, B. Ghidini³², P. Ghosh¹²⁸, S.K. Ghosh⁴, P. Gianotti⁶⁹, P. Giubellino³⁵, E. Gladysz-Dziadus¹¹³, P. Glässel⁹⁰, A. Gomez Ramirez⁴⁹, P. González-Zamora¹⁰, S. Gorbunov⁴⁰, L. Görlich¹¹³, S. Gotovac¹¹², L.K. Graczykowski¹³⁰, A. Grelli⁵⁴, A. Grigoras³⁵, C. Grigoras³⁵, V. Grigoriev⁷³, A. Grigoryan¹, S. Grigoryan⁶³, B. Grinyov³, N. Grion¹⁰⁷, J.F. Grosse-Oetringhaus³⁵, J.-Y. Grossiord¹²⁶, R. Grossi³⁵, F. Guber⁵³, R. Guernane⁶⁸, B. Guerzoni²⁷, M. Guilbaud¹²⁶, K. Gulbrandsen⁷⁷, H. Gulkanyan¹, M. Gumbo⁸⁶, T. Gunji¹²³, A. Gupta⁸⁷, R. Gupta⁸⁷, K. H. Khan¹⁵, R. Haake⁵¹, Ø. Haaland¹⁷, C. Hadjidakis⁴⁸, M. Haiduc⁵⁹, H. Hamagaki¹²³, G. Hamar¹³², L.D. Hanratty⁹⁹, A. Hansen⁷⁷, J.W. Harris¹³³, H. Hartmann⁴⁰, A. Harton¹³, D. Hatzifotiadou¹⁰², S. Hayashi¹²³, S.T. Heckel⁵⁰, M. Heide⁵¹, H. Helstrup³⁶, A. Herghelegiu⁷⁵, G. Herrera Corral¹¹, B.A. Hess³⁴, K.F. Hetland³⁶, B. Hippolyte⁵², J. Hladky⁵⁷, P. Hristov³⁵, M. Huang¹⁷, T.J. Humanic¹⁹, N. Hussain⁴², T. Hussain¹⁸, D. Hutter⁴⁰, D.S. Hwang²⁰, R. Ilkaev⁹⁶, I. Ilkiv⁷⁴, M. Inaba¹²⁴, G.M. Innocenti²⁶, C. Ionita³⁵,

M. Ippolitov⁹⁷, M. Irfan¹⁸, M. Ivanov⁹⁴, V. Ivanov⁸², A. Jacholkowski²⁸, P.M. Jacobs⁷¹, C. Jahnke¹¹⁶, H.J. Jang⁶⁵, M.A. Janik¹³⁰, P.H.S.Y. Jayaratna¹¹⁸, C. Jena²⁹, S. Jena¹¹⁸, R.T. Jimenez Bustamante⁶⁰, P.G. Jones⁹⁹, H. Jung⁴¹, A. Jusko⁹⁹, V. Kadyshevskiy⁶³, P. Kalinak⁵⁶, A. Kalweit³⁵, J. Kamin⁵⁰, J.H. Kang¹³⁴, V. Kaplin⁷³, S. Kar¹²⁸, A. Karasu Uysal⁶⁶, O. Karavichev⁵³, T. Karavicheva⁵³, E. Karpechev⁵³, U. Kebschull⁴⁹, R. Keidel¹³⁵, D.L.D. Keijdener⁵⁴, M. Keil SVN³⁵, M.M. Khan^{iii, 18}, P. Khan⁹⁸, S.A. Khan¹²⁸, A. Khanzadeev⁸², Y. Kharlov¹⁰⁹, B. Kileng³⁶, B. Kim¹³⁴, D.W. Kim^{41, 65}, D.J. Kim¹¹⁹, H. Kim¹³⁴, J.S. Kim⁴¹, M. Kim⁴¹, M. Kim¹³⁴, S. Kim²⁰, T. Kim¹³⁴, S. Kirsch⁴⁰, I. Kisel⁴⁰, S. Kiselev⁵⁵, A. Kisiel¹³⁰, G. Kiss¹³², J.L. Klay⁶, J. Klein⁹⁰, C. Klein-Bösing⁵¹, A. Kluge³⁵, M.L. Knichel⁹⁰, A.G. Knospe¹¹⁴, C. Kobdaj¹¹¹, M. Kofarago³⁵, M.K. Köhler⁹⁴, T. Kollegger⁴⁰, A. Kolojvari¹²⁷, V. Kondratiev¹²⁷, N. Kondratyeva⁷³, A. Konevskikh⁵³, V. Kovalenko¹²⁷, M. Kowalski¹¹³, S. Kox⁶⁸, G. Koyithatta Meethaleveedu⁴⁵, J. Kral¹¹⁹, I. Králik⁵⁶, A. Kravčáková³⁹, M. Krelina³⁸, M. Kretz⁴⁰, M. Krivda^{56, 99}, F. Krizek⁸⁰, E. Kryshen³⁵, M. Krzewicki^{94, 40}, V. Kučera⁸⁰, Y. Kucheriaev^{97, i}, T. Kugathasan³⁵, C. Kuhn⁵², P.G. Kuijer⁷⁸, I. Kulakov⁴⁰, J. Kumar⁴⁵, P. Kurashvili⁷⁴, A. Kurepin⁵³, A.B. Kurepin⁵³, A. Kuryakin⁹⁶, S. Kushpil⁸⁰, M.J. Kweon^{90, 47}, Y. Kwon¹³⁴, P. Ladron de Guevara⁶⁰, C. Lagana Fernandes¹¹⁶, I. Lakomov⁴⁸, R. Langoy¹²⁹, C. Lara⁴⁹, A. Lattuca²⁶, S.L. La Pointe¹⁰⁸, P. La Rocca²⁸, R. Lea²⁵, L. Leardini⁹⁰, G.R. Lee⁹⁹, I. Legrand³⁵, J. Lehnert⁵⁰, R.C. Lemmon⁷⁹, V. Lenti¹⁰¹, E. Leogrande⁵⁴, M. Leoncino²⁶, I. León Monzón¹¹⁵, P. Lévai¹³², S. Li^{7, 67}, J. Lien¹²⁹, R. Lietava⁹⁹, S. Linda²¹, V. Lindenstruth⁴⁰, C. Lippmann⁹⁴, M.A. Lisa¹⁹, H.M. Ljunggren³³, D.F. Lodato⁵⁴, P.I. Loenne¹⁷, V.R. Loggins¹³¹, V. Loginov⁷³, D. Lohner⁹⁰, C. Loizides⁷¹, X. Lopez⁶⁷, E. López Torres⁹, X.-G. Lu⁹⁰, P. Luettig⁵⁰, M. Lunardon²⁹, G. Luparello^{54, 25}, A. Maevskaya⁵³, M. Mager³⁵, D.P. Mahapatra⁵⁸, S.M. Mahmood²¹, A. Maire^{52, 90}, R.D. Majka¹³³, M. Malaev⁸², I. Maldonado Cervantes⁶⁰, L. Malinina^{iv, 63}, D. Mal'Kevich⁵⁵, P. Malzacher⁹⁴, A. Mamonov⁹⁶, L. Manceau¹⁰⁸, V. Manko⁹⁷, F. Manso⁶⁷, V. Manzari^{35, 101}, M. Marchisone²⁶, J. Mares⁵⁷, G.V. Margagliotti²⁵, A. Margotti¹⁰², A. Marín⁹⁴, C. Markert^{35, 114}, M. Marquard⁵⁰, I. Martashvili¹²¹, N.A. Martin⁹⁴, P. Martinengo³⁵, M.I. Martínez², G. Martínez García¹¹⁰, J. Martin Blanco¹¹⁰, Y. Martynov³, S. Masciocchi⁹⁴, M. Maseri²⁶, A. Masoni¹⁰³, L. Massacrier¹¹⁰, A. Mastroserio³², A. Matyja¹¹³, C. Mayer¹¹³, J. Mazer¹²¹, M.A. Mazzoni¹⁰⁶, D. McDonald¹¹⁸, F. Meddi²³, A. Menchaca-Rocha⁶¹, E. Meninno³⁰, J. Mercado Pérez⁹⁰, M. Meres³⁷, Y. Miake¹²⁴, K. Mikhaylov^{55, 63}, L. Milano³⁵, J. Milosevic^{v, 21}, L.M. Minervini^{101, 22}, A. Mischke⁵⁴, A.N. Mishra⁴⁶, D. Miśkowiec⁹⁴, J. Mitra¹²⁸, C.M. Mitu⁵⁹, J. Mlynarz¹³¹, N. Mohammadi⁵⁴, B. Mohanty^{128, 76}, L. Molnar⁵², L. Montaño Zetina¹¹, E. Montes¹⁰, M. Morando²⁹, D.A. Moreira De Godoy^{110, 116}, S. Moretto²⁹, A. Morreale¹¹⁰, A. Morsch³⁵, V. Muccifora⁶⁹, E. Mudnic¹¹², D. Mühlheim⁵¹, S. Muhuri¹²⁸, M. Mukherjee¹²⁸, H. Müller³⁵, M.G. Munhoz¹¹⁶, S. Murray^{86, 62}, L. Musa³⁵, J. Musinsky⁵⁶, B.K. Nandi⁴⁵, R. Nania¹⁰², E. Nappi¹⁰¹, M.U. Naru¹⁵, C. Nattrass¹²¹, K. Nayak⁷⁶, T.K. Nayak¹²⁸, S. Nazarenko⁹⁶, A. Nedosekin⁵⁵, M. Nicassio⁹⁴, M. Niculescu^{59, 35}, J. Niedziela³⁵, B.S. Nielsen⁷⁷, S. Nikolaev⁹⁷, S. Nikulin⁹⁷, V. Nikulin⁸², B.S. Nilsen⁸³, F. Noferini^{12, 102}, P. Nomokonov⁶³, G. Nooren⁵⁴, J. Norman¹²⁰, A. Nyanin⁹⁷, J. Nystrand¹⁷, H. Oeschler⁹⁰, S. Oh¹³³, S.K. Oh^{vi, 64, 41}, A. Okatan⁶⁶, T. Okubo⁴⁴, L. Olah¹³², J. Oleniacz¹³⁰, A.C. Oliveira Da Silva¹¹⁶, J. Onderwaater⁹⁴, C. Oppedisano¹⁰⁸, A. Ortiz Velasquez^{60, 33}, A. Oskarsson³³, J. Otwinowski^{94, 113}, K. Oyama⁹⁰, M. Ozdemir⁵⁰, P. Sahoo⁴⁶, Y. Pachmayer⁹⁰, M. Pachr³⁸, P. Pagano³⁰, G. Paić⁶⁰, C. Pajares¹⁶, S.K. Pal¹²⁸, A. Palmeri¹⁰⁴, D. Pant⁴⁵, V. Papikyan¹, G.S. Pappalardo¹⁰⁴, P. Pareek⁴⁶, W.J. Park⁹⁴, S. Parmar⁸⁴, A. Passfeld⁵¹, D.I. Patalakha¹⁰⁹, V. Paticchio¹⁰¹, B. Paul⁹⁸, T. Pawlak¹³⁰, T. Peitzmann⁵⁴, H. Pereira Da Costa¹⁴, E. Pereira De Oliveira Filho¹¹⁶, D. Peresunko⁹⁷, C.E. Pérez Lara⁷⁸, A. Pesci¹⁰², V. Peskov⁵⁰, Y. Pestov⁵, V. Petráček³⁸, M. Petran³⁸, M. Petris⁷⁵, M. Petrovici⁷⁵, C. Petta²⁸, S. Piano¹⁰⁷, M. Pikna³⁷, P. Pillot¹¹⁰, O. Pinazza^{102, 35}, L. Pinsky¹¹⁸, D.B. Piyarathna¹¹⁸, M. Płoskoń⁷¹, M. Planinic^{95, 125}, J. Pluta¹³⁰, S. Pochybova¹³², P.L.M. Podesta-Lerma¹¹⁵, M.G. Poghosyan^{83, 35}, E.H.O. Pohjoisaho⁴³, B. Polichtchouk¹⁰⁹, N. Poljak^{125, 95}, A. Pop⁷⁵, S. Porteboeuf-Houssais⁶⁷, J. Porter⁷¹, B. Potukuchi⁸⁷, S.K. Prasad^{131, 4}, R. Preghenella^{102, 12}, F. Prino¹⁰⁸, C.A. Pruneau¹³¹, I. Pshenichnov⁵³, M. Puccio¹⁰⁸, G. Puddu²⁴, P. Pujahari¹³¹, V. Punin⁹⁶, J. Putschke¹³¹, H. Qvigstad²¹, A. Rachevski¹⁰⁷, S. Raha⁴, S. Rajput⁸⁷, J. Rak¹¹⁹, A. Rakotozafindrabe¹⁴, L. Ramello³¹, R. Raniwala⁸⁸, S. Raniwala⁸⁸, S.S. Räsänen⁴³, B.T. Rascanu⁵⁰, D. Rathee⁸⁴, A.W. Rauf¹⁵, V. Razazi²⁴, K.F. Read¹²¹, J.S. Real⁶⁸, K. Redlich^{vii, 74}, R.J. Reed^{133, 131}, A. Rehman¹⁷, P. Reichelt⁵⁰, M. Reicher⁵⁴, F. Reidt^{90, 35}, R. Renfordt⁵⁰, A.R. Reolon⁶⁹, A. Reshetin⁵³, F. Rettig⁴⁰, J.-P. Revol³⁵, K. Reygers⁹⁰, V. Riabov⁸², R.A. Ricci⁷⁰, T. Richert³³, M. Richter²¹, P. Riedler³⁵, W. Riegler³⁵, F. Riggi²⁸, A. Rivetti¹⁰⁸, E. Rocco⁵⁴, M. Rodríguez Cahuantzi², A. Rodriguez Manso⁷⁸, K. Røed²¹, E. Rogochaya⁶³, S. Rohni⁸⁷, D. Rohr⁴⁰, D. Röhrich¹⁷, R. Romita^{120, 79}, F. Ronchetti⁶⁹, L. Ronflette¹¹⁰, P. Rosnet⁶⁷, A. Rossi³⁵, F. Roukoutakis⁸⁵, A. Roy⁴⁶, C. Roy⁵², P. Roy⁹⁸, A.J. Rubio Montero¹⁰, R. Ruf²⁵, R. Russo²⁶, E. Ryabinkin⁹⁷, Y. Ryabov⁸², A. Rybicki¹¹³, S. Sadovsky¹⁰⁹, K. Šafařík³⁵, B. Sahlmuller⁵⁰, R. Sahoo⁴⁶, S. Sahoo⁵⁸, P.K. Sahu⁵⁸, J. Saini¹²⁸, S. Sakai⁶⁹, C.A. Salgado¹⁶,

J. Salzwedel¹⁹, S. Sambyal⁸⁷, V. Samsonov⁸², X. Sanchez Castro⁵², F.J. Sánchez Rodríguez¹¹⁵, L. Šádor⁵⁶, A. Sandoval⁶¹, M. Sano¹²⁴, G. Santagati²⁸, D. Sarkar¹²⁸, E. Scapparone¹⁰², F. Scarlassara²⁹, R.P. Scharenberg⁹², C. Schiaua⁷⁵, R. Schicker⁹⁰, C. Schmidt⁹⁴, H.R. Schmidt³⁴, S. Schuchmann⁵⁰, J. Schukraft³⁵, M. Schulc³⁸, T. Schuster¹³³, Y. Schutz^{110,35}, K. Schwarz⁹⁴, K. Schweda⁹⁴, G. Sciol²⁷, E. Scomparin¹⁰⁸, R. Scott¹²¹, G. Segato²⁹, J.E. Seger⁸³, Y. Sekiguchi¹²³, I. Selyuzhenkov⁹⁴, K. Senosi⁶², J. Seo⁹³, E. Serradilla^{10,61}, A. Sevcenco⁵⁹, A. Shabetai¹¹⁰, G. Shabratova⁶³, R. Shahoyan³⁵, A. Shangaraev¹⁰⁹, A. Sharma⁸⁷, N. Sharma¹²¹, S. Sharma⁸⁷, K. Shigaki⁴⁴, K. Shtejer^{26,9}, Y. Sibiriak⁹⁷, S. Siddhanta¹⁰³, T. Siemiarczuk⁷⁴, D. Silvermyr⁸¹, C. Silvestre⁶⁸, G. Simatovic¹²⁵, R. Singaraju¹²⁸, R. Singh⁸⁷, S. Singha^{76,128}, V. Singhal¹²⁸, B.C. Sinha¹²⁸, T. Sinha⁹⁸, B. Sitar³⁷, M. Sitta³¹, T.B. Skaali²¹, K. Skjerdal¹⁷, M. Slupecki¹¹⁹, N. Smirnov¹³³, R.J.M. Snellings⁵⁴, C. Søgaard³³, R. Soltz⁷², J. Song⁹³, M. Song¹³⁴, F. Soramel²⁹, S. Sorensen¹²¹, M. Spacek³⁸, E. Spiriti⁶⁹, I. Sputowska¹¹³, M. Spyropoulou-Stassinaki⁸⁵, B.K. Srivastava⁹², J. Stachel⁹⁰, I. Stan⁵⁹, G. Stefanek⁷⁴, M. Steinpreis¹⁹, E. Stenlund³³, G. Steyn⁶², J.H. Stiller⁹⁰, D. Stocco¹¹⁰, P. Strmen³⁷, A.A.P. Suade¹¹⁶, T. Sugitate⁴⁴, C. Suire⁴⁸, M. Suleymanov¹⁵, R. Sultanov⁵⁵, M. Šumbera⁸⁰, T.J.M. Symons⁷¹, A. Szabo³⁷, A. Szanto de Toledo¹¹⁶, I. Szarka³⁷, A. Szczepankiewicz³⁵, M. Szymanski¹³⁰, J. Takahashi¹¹⁷, M.A. Tangaro³², J.D. Tapia Takaki^{viii,48}, A. Tarantola Peloni⁵⁰, A. Tarazona Martinez³⁵, M. Tariq¹⁸, M.G. Tarzila⁷⁵, A. Tauro³⁵, G. Tejeda Muñoz², A. Telesca³⁵, K. Terasaki¹²³, C. Terrevoli²⁴, J. Thäder⁹⁴, D. Thomas⁵⁴, R. Tieulent¹²⁶, A.R. Timmins¹¹⁸, A. Toia^{50,105}, V. Trubnikov³, W.H. Trzaska¹¹⁹, T. Tsuji¹²³, A. Tumkin⁹⁶, R. Turrisi¹⁰⁵, T.S. Tveter²¹, K. Ullaland¹⁷, A. Uras¹²⁶, G.L. Usai²⁴, M. Vajzer⁸⁰, M. Vala⁵⁶, L. Valencia Palomo⁶⁷, S. Vallero^{26,90}, T. Vanat⁸⁰, P. Vande Vyvre³⁵, J. Van Der Maarel⁵⁴, J.W. Van Hoorn³⁵, M. van Leeuwen⁵⁴, A. Vargas², M. Vargyas¹¹⁹, R. Varma⁴⁵, M. Vasileiou⁸⁵, A. Vasiliev⁹⁷, V. Vechernin¹²⁷, M. Veldhoen⁵⁴, A. Velure¹⁷, M. Venaruzzo⁷⁰, E. Vercellin²⁶, S. Vergara Limón², R. Vernet⁸, M. Verweij¹³¹, L. Vickovic¹¹², G. Viesti²⁹, J. Viinikainen¹¹⁹, Z. Vilakazi^{122,62}, O. Villalobos Baillie⁹⁹, A. Vinogradov⁹⁷, L. Vinogradov¹²⁷, Y. Vinogradov⁹⁶, T. Virgili³⁰, V. Vislavicius³³, Y.P. Viyogi¹²⁸, A. Vodopyanov⁶³, M.A. Völk⁹⁰, K. Voloshin⁵⁵, S.A. Voloshin¹³¹, G. Volpe³⁵, B. von Haller³⁵, I. Vorobyev¹²⁷, D. Vranic^{35,94}, J. Vrláková³⁹, B. Vulpescu⁶⁷, A. Vyushin⁹⁶, B. Wagner¹⁷, J. Wagner⁹⁴, V. Wagner³⁸, M. Wang^{7,110}, Y. Wang⁹⁰, D. Watanabe¹²⁴, M. Weber^{118,35}, S.G. Weber⁹⁴, J.P. Wessels⁵¹, U. Westerhoff⁵¹, J. Wiechula³⁴, J. Wikne²¹, M. Wilde⁵¹, G. Wilk⁷⁴, J. Wilkinson⁹⁰, M.C.S. Williams¹⁰², B. Windelband⁹⁰, M. Winn⁹⁰, C.G. Yaldo¹³¹, Y. Yamaguchi¹²³, H. Yang⁵⁴, P. Yang⁷, S. Yang¹⁷, S. Yano⁴⁴, S. Yasnopolskiy⁹⁷, Z. Yin⁷, I.-K. Yoo⁹³, I. Yushmanov⁹⁷, A. Zaborowska¹³⁰, V. Zaccolo⁷⁷, A. Zaman¹⁵, C. Zampolli¹⁰², S. Zaporozhets⁶³, A. Zarochentsev¹²⁷, P. Závada⁵⁷, N. Zaviyalov⁹⁶, H. Zbroszczyk¹³⁰, I.S. Zgura⁵⁹, M. Zhalov⁸², H. Zhang⁷, X. Zhang^{7,71}, Y. Zhang⁷, C. Zhao²¹, N. Zhigareva⁵⁵, D. Zhou⁷, F. Zhou⁷, Y. Zhou⁵⁴, Zhou, Zhuo¹⁷, H. Zhu⁷, J. Zhu^{7,110}, X. Zhu⁷, A. Zichichi^{12,27}, A. Zimmermann⁹⁰, M.B. Zimmermann^{51,35}, G. Zinovjev³, Y. Zoccarato¹²⁶, M. Zyzak⁴⁰

Affiliation notes

ⁱ Deceased

ⁱⁱ Also at: St. Petersburg State Polytechnical University

ⁱⁱⁱ Also at: Department of Applied Physics, Aligarh Muslim University, Aligarh, India

^{iv} Also at: M.V. Lomonosov Moscow State University, D.V. Skobeltsyn Institute of Nuclear Physics, Moscow, Russia

^v Also at: University of Belgrade, Faculty of Physics and "Vinča" Institute of Nuclear Sciences, Belgrade, Serbia

^{vi} Permanent Address: Permanent Address: Konkuk University, Seoul, Korea

^{vii} Also at: Institute of Theoretical Physics, University of Wrocław, Wrocław, Poland

^{viii} Also at: University of Kansas, Lawrence, KS, United States

Collaboration Institutes

¹ A.I. Alikhanyan National Science Laboratory (Yerevan Physics Institute) Foundation, Yerevan, Armenia

² Benemérita Universidad Autónoma de Puebla, Puebla, Mexico

³ Bogolyubov Institute for Theoretical Physics, Kiev, Ukraine

⁴ Bose Institute, Department of Physics and Centre for Astroparticle Physics and Space Science (CAPSS), Kolkata, India

⁵ Budker Institute for Nuclear Physics, Novosibirsk, Russia

⁶ California Polytechnic State University, San Luis Obispo, CA, United States

- ⁷ Central China Normal University, Wuhan, China
⁸ Centre de Calcul de l'IN2P3, Villeurbanne, France
⁹ Centro de Aplicaciones Tecnológicas y Desarrollo Nuclear (CEADEN), Havana, Cuba
¹⁰ Centro de Investigaciones Energéticas Medioambientales y Tecnológicas (CIEMAT), Madrid, Spain
¹¹ Centro de Investigación y de Estudios Avanzados (CINVESTAV), Mexico City and Mérida, Mexico
¹² Centro Fermi - Museo Storico della Fisica e Centro Studi e Ricerche “Enrico Fermi”, Rome, Italy
¹³ Chicago State University, Chicago, USA
¹⁴ Commissariat à l'Energie Atomique, IRFU, Saclay, France
¹⁵ COMSATS Institute of Information Technology (CIIT), Islamabad, Pakistan
¹⁶ Departamento de Física de Partículas and IGFAE, Universidad de Santiago de Compostela, Santiago de Compostela, Spain
¹⁷ Department of Physics and Technology, University of Bergen, Bergen, Norway
¹⁸ Department of Physics, Aligarh Muslim University, Aligarh, India
¹⁹ Department of Physics, Ohio State University, Columbus, OH, United States
²⁰ Department of Physics, Sejong University, Seoul, South Korea
²¹ Department of Physics, University of Oslo, Oslo, Norway
²² Dipartimento di Elettrotecnica ed Elettronica del Politecnico, Bari, Italy
²³ Dipartimento di Fisica dell'Università 'La Sapienza' and Sezione INFN Rome, Italy
²⁴ Dipartimento di Fisica dell'Università and Sezione INFN, Cagliari, Italy
²⁵ Dipartimento di Fisica dell'Università and Sezione INFN, Trieste, Italy
²⁶ Dipartimento di Fisica dell'Università and Sezione INFN, Turin, Italy
²⁷ Dipartimento di Fisica e Astronomia dell'Università and Sezione INFN, Bologna, Italy
²⁸ Dipartimento di Fisica e Astronomia dell'Università and Sezione INFN, Catania, Italy
²⁹ Dipartimento di Fisica e Astronomia dell'Università and Sezione INFN, Padova, Italy
³⁰ Dipartimento di Fisica ‘E.R. Caianiello’ dell'Università and Gruppo Collegato INFN, Salerno, Italy
³¹ Dipartimento di Scienze e Innovazione Tecnologica dell'Università del Piemonte Orientale and Gruppo Collegato INFN, Alessandria, Italy
³² Dipartimento Interateneo di Fisica ‘M. Merlin’ and Sezione INFN, Bari, Italy
³³ Division of Experimental High Energy Physics, University of Lund, Lund, Sweden
³⁴ Eberhard Karls Universität Tübingen, Tübingen, Germany
³⁵ European Organization for Nuclear Research (CERN), Geneva, Switzerland
³⁶ Faculty of Engineering, Bergen University College, Bergen, Norway
³⁷ Faculty of Mathematics, Physics and Informatics, Comenius University, Bratislava, Slovakia
³⁸ Faculty of Nuclear Sciences and Physical Engineering, Czech Technical University in Prague, Prague, Czech Republic
³⁹ Faculty of Science, P.J. Šafárik University, Košice, Slovakia
⁴⁰ Frankfurt Institute for Advanced Studies, Johann Wolfgang Goethe-Universität Frankfurt, Frankfurt, Germany
⁴¹ Gangneung-Wonju National University, Gangneung, South Korea
⁴² Gauhati University, Department of Physics, Guwahati, India
⁴³ Helsinki Institute of Physics (HIP), Helsinki, Finland
⁴⁴ Hiroshima University, Hiroshima, Japan
⁴⁵ Indian Institute of Technology Bombay (IIT), Mumbai, India
⁴⁶ Indian Institute of Technology Indore, Indore (IITI), India
⁴⁷ Inha University, Incheon, South Korea
⁴⁸ Institut de Physique Nucléaire d'Orsay (IPNO), Université Paris-Sud, CNRS-IN2P3, Orsay, France
⁴⁹ Institut für Informatik, Johann Wolfgang Goethe-Universität Frankfurt, Frankfurt, Germany
⁵⁰ Institut für Kernphysik, Johann Wolfgang Goethe-Universität Frankfurt, Frankfurt, Germany
⁵¹ Institut für Kernphysik, Westfälische Wilhelms-Universität Münster, Münster, Germany
⁵² Institut Pluridisciplinaire Hubert Curien (IPHC), Université de Strasbourg, CNRS-IN2P3, Strasbourg, France
⁵³ Institute for Nuclear Research, Academy of Sciences, Moscow, Russia
⁵⁴ Institute for Subatomic Physics of Utrecht University, Utrecht, Netherlands
⁵⁵ Institute for Theoretical and Experimental Physics, Moscow, Russia
⁵⁶ Institute of Experimental Physics, Slovak Academy of Sciences, Košice, Slovakia
⁵⁷ Institute of Physics, Academy of Sciences of the Czech Republic, Prague, Czech Republic

- 58 Institute of Physics, Bhubaneswar, India
59 Institute of Space Science (ISS), Bucharest, Romania
60 Instituto de Ciencias Nucleares, Universidad Nacional Autónoma de México, Mexico City, Mexico
61 Instituto de Física, Universidad Nacional Autónoma de México, Mexico City, Mexico
62 iThemba LABS, National Research Foundation, Somerset West, South Africa
63 Joint Institute for Nuclear Research (JINR), Dubna, Russia
64 Konkuk University, Seoul, South Korea
65 Korea Institute of Science and Technology Information, Daejeon, South Korea
66 KTO Karatay University, Konya, Turkey
67 Laboratoire de Physique Corpusculaire (LPC), Clermont Université, Université Blaise Pascal, CNRS-IN2P3, Clermont-Ferrand, France
68 Laboratoire de Physique Subatomique et de Cosmologie, Université Grenoble-Alpes, CNRS-IN2P3, Grenoble, France
69 Laboratori Nazionali di Frascati, INFN, Frascati, Italy
70 Laboratori Nazionali di Legnaro, INFN, Legnaro, Italy
71 Lawrence Berkeley National Laboratory, Berkeley, CA, United States
72 Lawrence Livermore National Laboratory, Livermore, CA, United States
73 Moscow Engineering Physics Institute, Moscow, Russia
74 National Centre for Nuclear Studies, Warsaw, Poland
75 National Institute for Physics and Nuclear Engineering, Bucharest, Romania
76 National Institute of Science Education and Research, Bhubaneswar, India
77 Niels Bohr Institute, University of Copenhagen, Copenhagen, Denmark
78 Nikhef, National Institute for Subatomic Physics, Amsterdam, Netherlands
79 Nuclear Physics Group, STFC Daresbury Laboratory, Daresbury, United Kingdom
80 Nuclear Physics Institute, Academy of Sciences of the Czech Republic, Řež u Prahy, Czech Republic
81 Oak Ridge National Laboratory, Oak Ridge, TN, United States
82 Petersburg Nuclear Physics Institute, Gatchina, Russia
83 Physics Department, Creighton University, Omaha, NE, United States
84 Physics Department, Panjab University, Chandigarh, India
85 Physics Department, University of Athens, Athens, Greece
86 Physics Department, University of Cape Town, Cape Town, South Africa
87 Physics Department, University of Jammu, Jammu, India
88 Physics Department, University of Rajasthan, Jaipur, India
89 Physik Department, Technische Universität München, Munich, Germany
90 Physikalisches Institut, Ruprecht-Karls-Universität Heidelberg, Heidelberg, Germany
91 Politecnico di Torino, Turin, Italy
92 Purdue University, West Lafayette, IN, United States
93 Pusan National University, Pusan, South Korea
94 Research Division and ExtreMe Matter Institute EMMI, GSI Helmholtzzentrum für Schwerionenforschung, Darmstadt, Germany
95 Rudjer Bošković Institute, Zagreb, Croatia
96 Russian Federal Nuclear Center (VNIIEF), Sarov, Russia
97 Russian Research Centre Kurchatov Institute, Moscow, Russia
98 Saha Institute of Nuclear Physics, Kolkata, India
99 School of Physics and Astronomy, University of Birmingham, Birmingham, United Kingdom
100 Sección Física, Departamento de Ciencias, Pontificia Universidad Católica del Perú, Lima, Peru
101 Sezione INFN, Bari, Italy
102 Sezione INFN, Bologna, Italy
103 Sezione INFN, Cagliari, Italy
104 Sezione INFN, Catania, Italy
105 Sezione INFN, Padova, Italy
106 Sezione INFN, Rome, Italy
107 Sezione INFN, Trieste, Italy
108 Sezione INFN, Turin, Italy
109 SSC IHEP of NRC Kurchatov institute, Protvino, Russia
110 SUBATECH, Ecole des Mines de Nantes, Université de Nantes, CNRS-IN2P3, Nantes, France

- ¹¹¹ Suranaree University of Technology, Nakhon Ratchasima, Thailand
¹¹² Technical University of Split FESB, Split, Croatia
¹¹³ The Henryk Niewodniczanski Institute of Nuclear Physics, Polish Academy of Sciences, Cracow, Poland
¹¹⁴ The University of Texas at Austin, Physics Department, Austin, TX, USA
¹¹⁵ Universidad Autónoma de Sinaloa, Culiacán, Mexico
¹¹⁶ Universidade de São Paulo (USP), São Paulo, Brazil
¹¹⁷ Universidade Estadual de Campinas (UNICAMP), Campinas, Brazil
¹¹⁸ University of Houston, Houston, TX, United States
¹¹⁹ University of Jyväskylä, Jyväskylä, Finland
¹²⁰ University of Liverpool, Liverpool, United Kingdom
¹²¹ University of Tennessee, Knoxville, TN, United States
¹²² University of the Witwatersrand, Johannesburg, South Africa
¹²³ University of Tokyo, Tokyo, Japan
¹²⁴ University of Tsukuba, Tsukuba, Japan
¹²⁵ University of Zagreb, Zagreb, Croatia
¹²⁶ Université de Lyon, Université Lyon 1, CNRS/IN2P3, IPN-Lyon, Villeurbanne, France
¹²⁷ V. Fock Institute for Physics, St. Petersburg State University, St. Petersburg, Russia
¹²⁸ Variable Energy Cyclotron Centre, Kolkata, India
¹²⁹ Vestfold University College, Tønsberg, Norway
¹³⁰ Warsaw University of Technology, Warsaw, Poland
¹³¹ Wayne State University, Detroit, MI, United States
¹³² Wigner Research Centre for Physics, Hungarian Academy of Sciences, Budapest, Hungary
¹³³ Yale University, New Haven, CT, United States
¹³⁴ Yonsei University, Seoul, South Korea
¹³⁵ Zentrum für Technologietransfer und Telekommunikation (ZTT), Fachhochschule Worms, Worms, Germany